FLUME MEASUREMENTS OF EROSION CHARACTERISTICS OF SOILS AT BRIDGE FOUNDATIONS IN GEORGIA

A Thesis
Presented to
The Academic Faculty

by

Hernan Ricardo Navarro

In Partial Fulfillment
of the Requirements for the Degree
Master of Science in Civil Engineering

Georgia Institute of Technology
April 2004

FLUME MEASUREMENTS OF EROSION CHARACTERISTICS OF SOILS AT BRIDGE FOUNDATIONS IN GEORGIA

Approved:

_____
Terry Sturm, Advisor

_____
Carlos Santamarina

_____
Paul Work

Date Approved 4/27/2004

ACKNOWLEDGEMENTS

I am sincerely grateful to my advisor Dr. Terry Sturm for his trust, motivation and support. I appreciate the interest of Dr. Carlos Santamarina and Dr. Paul Work in this study and I am thankful for their comments and ideas. I would also want to thank Andy Udell for his help in flume measurements and Joshua Robinson for his assistance during the writing of this thesis. I am also thankful for the support of Robbie Frizzell and the team from J. B. Trimble Inc.

This project was funded by the Georgia Department of Transportation (GDOT). I appreciate their financial support.

TABLE OF CONTENTS

LIST OF FIGURES

LIST OF TABLES

LIST OF SYMBOLS

a	erosion rate constant exponential case
A	constant, Roberts et al. (1998)
A_h	Hamaker constant = 10^{-20} J
$Area$	cross sectional area of the Shelby tube
b_0	constant, Donat (1929)
b_1	constant, Donat (1929)
b_2	constant, Donat (1929)
c_0	ionic concentration of the pore fluid
d	particle diameter
d_{50}	median particle diameter
d_*	dimensionless particle diameter
e	soil void ratio
e_0	1.602x10^{-19} C is the electron charge
F	Froude number
f	friction factor
f_b	bed friction factor
f_w	wall friction factor
F_{pp}	Force between parallel platy particles
F_{sp}	Force between sphere and parallel particle
F_{ss}	Force between two spheres
$Fines$	decimal fraction of fine material
Gs	specific gravity
E	erosion rate
k_s	sand-grain roughness of the flume
m	constant, Roberts et al. (1998)
M	erosion rate constant linear case
M_{ash}	mass of ash
M_c	mass of container
M_{cs}	mass of container and oven dry specimen
M_{cws}	mass of container and wet specimen
M_s	mass of soil particles
M_w	mass of water
n	constant, Roberts et al. (1998)
n	Manning's roughness coefficient
n_b	bed Manning's roughness coefficient
OM	organic matter content
q_t	total volumetric sediment discharge per unit width
r	distance between edge and face
R	gas constant
R	hydraulic radius
R	radius of the sphere for the sphere and platy particle case
R_1	radius of sphere one for the two spheres case
R_2	radius of sphere two for the two sphere case

R_b	bed hydraulic radius
R_{DL}	repulsion force per unit area for long interparticle distances
Re	Reynolds number
S	slope
s_1	erosion rate constant linear case
s_2	erosion rate constant exponential case
T	temperature
u	thickness of the double layer
U	buoyancy
V	mean velocity
V_T	total volume of soil particles and voids
W	weight
WC	water content
y	flow depth
z	ionic valence
Δt	time interval over which the erosion occurs
Δy	vertical displacement of the sediment
γ_w	water specific weight
ε_0	8.85×10^{-12} F/m is the permittivity of vacuum
κ'	real relative permittivity of the medium
ν	viscosity of the water
ρ	water density
ρ_{bulk}	soil bulk density
ρ_{dry}	soil dry density
τ_0	applied shear stress
τ_b	applied shear stress
τ_c	critical shear stress
τ_{*c}	Shields parameter

SUMMARY

Shelby tube sediment samples collected from the foundations of ten (10) bridges located in the state of Georgia were tested in the laboratory to find their erosional behavior and the correlation of erosion parameters with sediment properties in order to improve the prediction of scour around bridge foundations. These sites were spatially distributed in order to fall into different major river basins and in different physiographic regions. A description of the Valley and Ridge, Blue Ridge, Piedmont, and Coastal Plain physiographic regions of Georgia is included, and the erosion parameters found from flume measurements are associated with their respective regions. Flume measurements were performed using a rectangular, tilting, recirculating flume located in the hydraulics lab in the School of Civil and Environmental Engineering at Georgia Tech. Velocities up to 1.7 m/s and bed shear stresses up to 21 Pa can be achieved in the flume. Regression analysis was performed on erosion rates as a function of applied shear stress to determine the parameters of the erosion function. The resulting parameters, the critical shear stress and the erosion rate constant, were correlated with soil properties and physiographic regions.

Experimental methodology was chosen to approach this problem because the involvement of interparticle forces for fine-grained materials makes it difficult to deal with the erosion phenomenon through other means. Nevertheless, analytical description of the erosion phenomenon was included in order to provide a better understanding of it.

Linear, exponential and power regression mathematical models for erosion rate were compared, and the two best-fit regression models of erosion rate as a function of shear stress are proposed to formulate a methodology intended to characterize the behavior of a soil exposed to erosive flow conditions. One of them is a linear model to calculate critical shear stresses and low erosion rates. The second model, which is exponential, has the advantage of describing the erosion rate response for a wider range of shear stress values. It is shown that one of the most relevant predictors for the critical shear stress and erosion rate constant in the regression models is the fine material content present in the sample, which is an indirect indicator of the contribution of interparticle forces to the erosion process. Applying the described methodology, a more case-specific calculation of the erosion at bridge foundations can be performed taking into account the actual material in situ.

CHAPTER I

INTRODUCTION

When a river flow is disturbed from its natural conditions by changes in hydrologic or sediment equilibrium, contractions of the flow cross section, or obstructions such as those caused by bridge foundations, the original shear stresses can be magnified significantly resulting in erosion. There are three main classes of erosion on river beds: general degradation, contraction scour and local scour. General degradation is caused by engineering works such as dams and dredging, and it is manifested along the river profile over an extensive longitudinal distance. Another class of erosion is contraction scour, which occurs across the entire streambed as a result of any contraction of the main channel of the river such as that caused by a bridge. The final class of erosion is called local scour. Local scour occurs due to flow obstruction by bridge piers, abutments or spurs. The joint action of local and contraction scour are the main causes of the failure of hydraulic structures such as bridges.

River beds at bridge sites are subject to complex flow patterns created by the flow around the foundations of the structure. Increased velocities and the formation of horseshoe vortices around the base of the foundations (piers and abutments) are the two main hydrodynamic processes that produce forces on the surface particles of the material that forms the bed of the river. Both mechanisms can be related to bed shear stresses. In resistance to the hydrodynamic forces, sediments have interparticle forces, either due to

gravity in the case of coarse sediments, or to electric charge interaction and molecular attraction in fine sediments. If the interparticle forces are overcome, erosion or scour occurs. In addition, when erosion appears there will be deposition of the eroded material downstream. Both phenomena have an impact on bridge foundations and on the natural conditions of the river or stream.

According to the Hydraulic Engineering Circular 18 (HEC 18) by the Federal Highway Administration (Richardson et al., 2001), the most common cause of bridge failure is floods and inside that group of flood damages, the most common cause is scouring of bridge foundations. An example of the damages that can be caused by bridge scour is illustrated by the spring floods of 1987 during which 17 bridges were damaged or destroyed in New York and New England. The Mississippi River flooding of 1993 resulted in 23 bridge failures with total damages of $15 million, with bridge abutment scour as the main source of failure. Tropical storm Alberto hit Georgia in 1994 and was responsible for approximately $130 million in damages to the highway system (Richardson et al. 2001).

The properties of the sediment being eroded will dictate the resistance to erosion or scour. Evaluating the total resisting force of any sediment, especially fine sediments, is very difficult so that it usually has to be approached by experimental means. The reason is that resisting forces depend on many sediment parameters and the variability of each parameter introduces considerable uncertainty in erosion indices. However, theoretical approaches can narrow the list of variables, leaving the parameters that most significantly

influence the erosion phenomenon. Also, the geographic setting can offer broader information about the material encountered in a given area. It is the objective of this research to combine experimental measurements of sediment properties and their geographic setting to produce more effective estimates of erodibility relative to the protection of bridge foundations.

The experimental part of this research is performed utilizing a laboratory recirculating flume, which is adapted to test the erodibility of sediment samples taken in the field using thin-walled tubes (Shelby tubes). Recirculating flumes have been used to perform research on erosion in addition to annular flumes and impinging jets. Thin-walled tube sampling is one of the most common ways of sampling in geotechnical engineering and provides for the experiments a fairly undisturbed material that is an excellent sample of the material in situ.

A review of the literature on this topic is given in Chapter II. The experimental approach and description of equipment and measurement devices is detailed in Chapter III. Chapter IV contains the results obtained and discussion. Finally, chapter V includes the conclusions and recommendation for future research.

CHAPTER II

LITERATURE REVIEW

2.1 Sediment Properties

The size of the particles being eroded is the principal factor that influences the type of forces involved in resisting erosion. For coarse sediments with low content of fine particles (smaller than 76 microns) gravity forces govern the process. Alternatively, when fine sizes are present in the bed material, additional forces become important. For instance, for particle sizes smaller than 10 microns or clay sizes, electrical forces make their appearance. In addition, the particle-fluid interaction cannot be disregarded. The ionic concentration and pH of the fluid affect particle charges; therefore the erosion process becomes dependent on the chemistry of the pore water.

As the particles get smaller, electrical forces have more effect on the erosion resistance because electrical forces are highly dependent on the particle's specific surface area, which is defined as the surface area per unit volume or mass of the particle. Given that specific surface area increases as the size decreases, and that it is greater for platy particles than for spherical particles, an abrupt change in the behavior of the forces takes place as the size changes from silty to clay-size material. Silty material is the result of mechanical weathering and therefore maintains a rounded shape. On the other hand, clay has platy structures with high values of specific surface area. As a result, the interparticle forces that resist the hydrodynamic drag force and erosion include the gravitational force, Coulombian attraction, van der Waals attraction and double layer repulsion. Short range

forces, such as hydration forces and Born repulsion, may also be important in determining the net overall attractive or repulsive force between clay particles (Mahmood et al. 2001). Capillary forces are ignored due to the high saturation conditions of bed material. A further review of the relevant interparticle forces is presented next (following Santamarina 2001)

The gravitational force has two components; weight W and buoyancy U. For spherical particles these forces are given by

$$W = \frac{1}{6} \cdot \pi \cdot G_s \cdot \gamma_w \cdot d^3 \tag{2.1}$$

$$U = \frac{1}{6} \cdot \pi \cdot \gamma_w \cdot d^3 \tag{2.2}$$

where d = particle diameter; G_s = specific gravity; and γ_w = water specific weight. The submerged weight, W_s is given by

$$W_s = W - U \tag{2.3}$$

The hydrodynamic force or drag force (D) is produced by a viscous fluid moving around a particle and consists of both surface drag and form drag components. This force is given in general by

$$D = C_D \rho A_f \frac{V^2}{2} \tag{2.4}$$

in which C_D = coefficient of drag; ρ = the density of the water; V = the flow velocity; and A_f = frontal area of the particle. The movement of particles is produced when the drag force (D) overcomes the submerged weight (W_s). The hydrodynamic force in the sediment transport literature is represented by the applied shear stress (τ), or force per unit surface area. The applied shear stress (τ) for open channel uniform flow is given by

$$\tau = \gamma_w \cdot R \cdot S \tag{2.5}$$

in which γ_w = water specific weight; R = hydraulic radius; and S = slope. Now, the threshold of movement is defined by the critical shear stress, τ_c, which can be given as a function of (following Sturm 2001)

$$\tau_c = f_1(\gamma_s - \gamma_w, d, \rho, \mu) \tag{2.6}$$

in which γ_s - γ_w = submerged specific weight; d = particle diameter; ρ = water density; and μ = water dynamic viscosity. Dimensional analysis of Equation 2.6 results in

$$\tau_{*c} = \frac{\tau_c}{(\gamma_s - \gamma_w) \cdot d} = f_2\left(\mathrm{Re}_{*c} = \frac{(\tau_c / \rho)^{1/2} \cdot d}{\nu}\right) \tag{2.7}$$

in which ν = kinematic viscosity; τ_{*c} = Shields Parameter; and Re_{*c} = critical boundary or particle Reynolds number. These last two parameters were presented by Shields (1936)

for the beginning of sediment motion in his widely known Shields Diagram. The first parameter (τ_{*c}) can be interpreted as the ratio of the hydrodynamic force per unit area to the gravitational force per unit volume. The second parameter (Re_{*c}) is roughly the ratio of the particle diameter to the thickness of the viscous sublayer. In the definition of the last two parameters the diameter and the critical shear stress are included, which impedes the direct calculation of the critical shear stress for a given diameter. The introduction of a third dimensionless parameter, given by $[0.1\mathbf{Re}_{*c}^{2}/\tau_{*c}]^{1/2}$, eliminates this restriction. The result of that analysis can be given in the form (Julien 1995)

$$\tau_{*c} = f_3\left(d_* = \left[\frac{(SG-1)\cdot g\cdot d^3}{\nu^2}\right]^{1/3}\right) \tag{2.8}$$

in which d_* = dimensionless particle diameter and SG = specific gravity. The graph is shown in Figure 2-1.

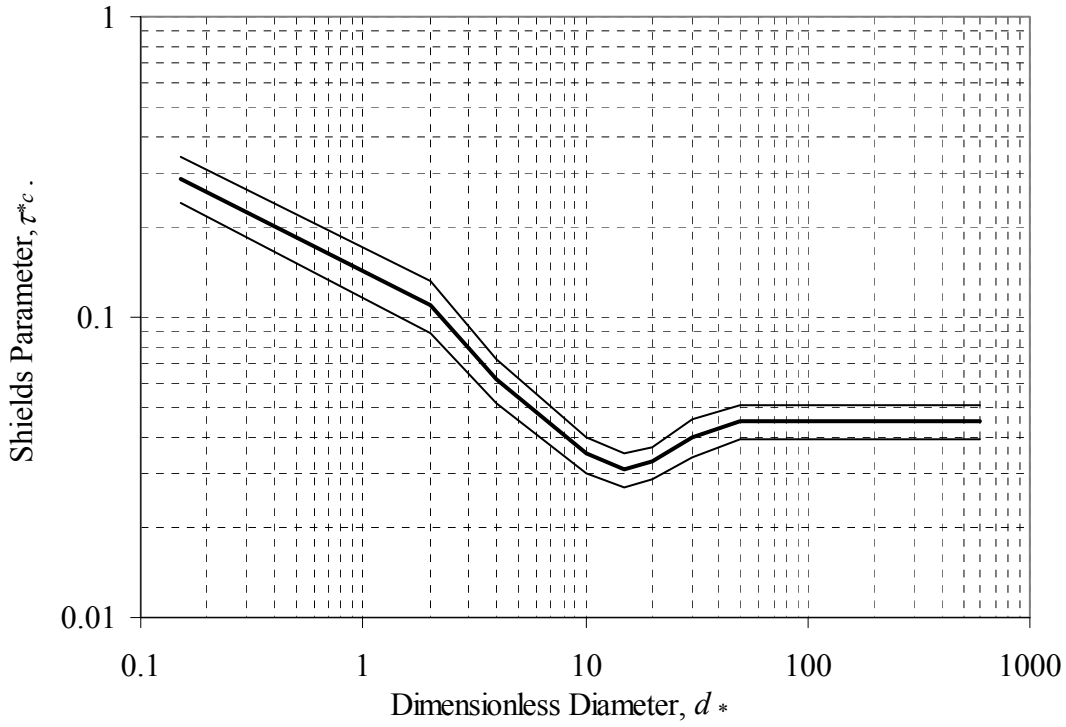

Figure 2-1. Shields diagram for direct determination of critical shear stress (after Sturm 2001).

For fine-grained materials, in addition to gravitational forces opposing the movement, interparticle forces start to act. Among these can be mentioned the Coulombian attraction, the van der Waals attraction and the double layer repulsion.

Coulombian attraction acts when there are counter charges interacting. Edges of clay particles that have a positive charge are attracted to the negative face of the mineral. The force is a function of the two charges q_1 and q_2 and of the distance r between the edge of a particle and the face of the other as given by

$$F = \frac{1}{4\pi \cdot \varepsilon_0 \cdot \kappa'} \cdot \frac{q_1 q_2}{r^2} = \frac{e_0^2}{4\pi \cdot \varepsilon_0 \cdot \kappa'} \cdot \frac{z_1 z_2}{r^2} \qquad (2.9)$$

in which $\varepsilon_0 = 8.85\text{x}10^{-12}$ F/m is the permittivity of vacuum; κ' = real relative permittivity of the medium; $e_0 = 1.602\text{x}10^{-19}$ C is the electron charge; z = ionic valence; and r = distance between edge and face.

Van der Waals attraction is a function of the Hamaker constant that is a measure of the permittivity of the fluid present between the particles. The closer the particles can move towards each other, the stronger that this force will be. Its value depends on the shape of the interacting particles as expressed by

$$F_{pp} = -\frac{A_h}{6\pi \cdot r^3} (N/m^2) \quad \textit{Parallel Platy Particles} \qquad (2.10)$$

$$F_{ss} = -\frac{A_h}{6\pi \cdot r^2} \cdot \frac{R_1 \cdot R_2}{R_1 + R_2} (N/m^2) \quad \textit{Two Spheres} \qquad (2.11)$$

$$F_{sp} = -\frac{A_h}{6\pi \cdot r^2} \cdot R\,(N/m^2) \quad \textit{Sphere and Platy Particle} \qquad (2.12)$$

in which A_h = Hamaker constant = 10^{-20} J; r = distance between edges or faces; R_1 = radius of sphere one for the two-spheres case; R_2 = radius of sphere two for the two-sphere case; and R = radius of the sphere for the sphere and platy-particle case.

The double layer repulsion force makes erosion more likely. This force acts to cause particle repulsion, making erosion by hydrodynamic forces easier. It depends on the ionic concentration of the environment more than any other factor. As a result of this dependence, when ionic concentration changes, this force changes and affects the equilibrium of the system. Coulombian and van der Waals forces will redistribute to form a new equilibrium state with a new particle arrangement. Israelachvili (1992) estimated the repulsion force per unit area R_{DL} for long interparticle distances as

$$R_{DL} = 64 \cdot \left(R \cdot T \cdot c_0\right) \cdot e^{-r/u} \tag{2.13}$$

where R = gas constant; u = thickness of the double layer; T = temperature; c_0 = ionic concentration of the pore fluid; and r = distance between edges and faces.

The relative contribution of the interparticle forces depends on the size and structure of sediments. For example, considering two relevant forces, gravitational and van der Waals, it can be seen in Figure 2-2 that particle weight is overwhelmed by the van der Waals force for particles smaller than 60 microns. Thus, the applied hydrodynamic drag force, which is a combination of surface and form drag as well as turbulent bursts near the bed, must overcome not only the gravitational forces but also the interparticle forces for fine-grained sediments. In this example, the forces are calculated considering spherical particles and particles separated 30 Angstroms for the van der Waals attraction.

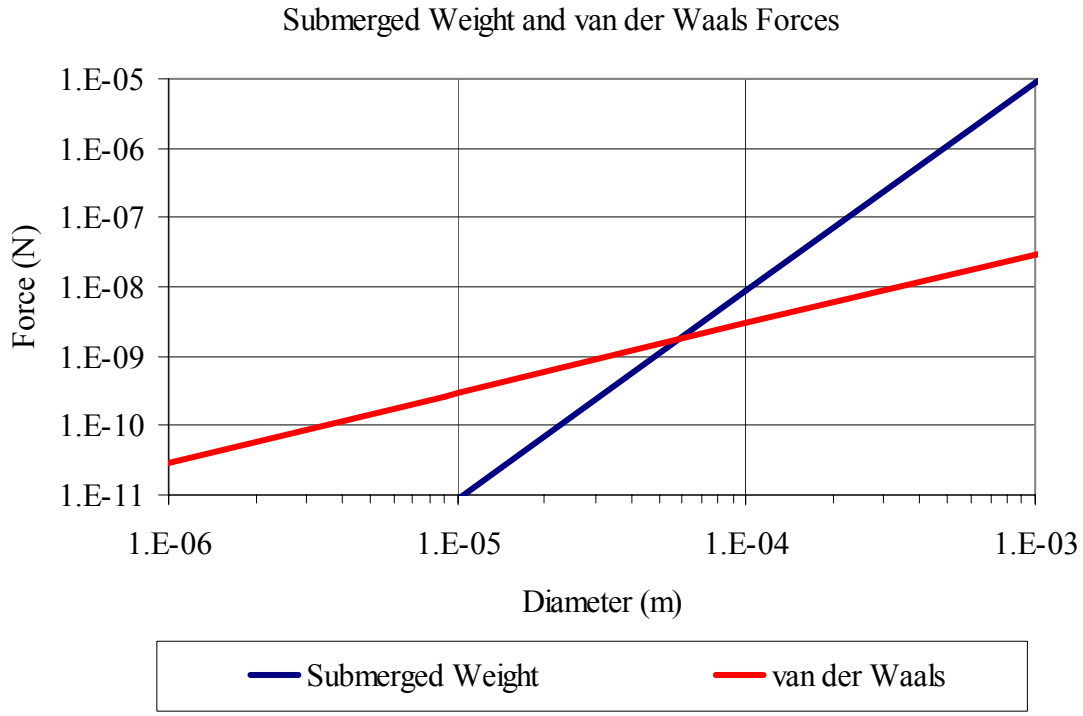

Figure 2-2. Relative contribution of submerged weight and van der Waals forces.

The arrangement of the sediment particles is an important determinant of erosion resistance. Sediments that form a well-arranged structure will be stronger than sediments that do not. The arrangement of particles depends on pH and ionic concentration conditions present when they are deposited. Fine-grained particles have four main associations: Edge-to-Face, Edge-to-Edge, Face-to-Face and shifted Face-to-Face. Edge-to-Face (E-F) arrangements are governed by Coulombian forces presented by the contrary charge of the faces and edges of the particles. Face-to-Face (F-F) arrangements are present when sedimentation occurs at high concentrations and the van der Waals force prevails over the double layer repulsion. Edge-to-Edge (E-E) are transition

arrangements of the last descriptions given that there is not a dominant force that governs the final structure. See Table 2-1, where the Edge-to-Face and Edge-to-Edge associations are referred to as flocculation, and the Face-to-Face and shifted Face-to-Face are referred to as aggregation (van Olphen 1977).

Table 2-1. Particle association in fine-grained materials (after van Olphen 1977)

Flocculation	Edge-to-Face		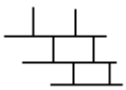
	Edge-to-Edge		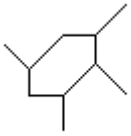
Aggregation	Face-to-Face		
	Shifted Face-to-Face		

Ravisangar et al. (2001) analyzed the influence of sediment pH on bed structure formation and on initial erosion rates in flume experiments on kaolinite sediment. For different pH conditions, kaolinite sediments have different bed structures and therefore different values of bulk density and water content. Initial erosion rates were measured for those structures with the following results. For pH conditions below 5.5, Edge-to-Face associations predominate. As the pH increases, the bed structure becomes weaker, corresponding to Edge-to-Edge associations dominating the structure. At pH conditions

above 7, the sediment particles associate as Face-to-Face increasing resistance to erosion. In terms of erosion resistance, the strongest associations were E-F and F-F, while erosional strength was less in the transition stage.

Mahmood et al. (2001) performed experiments on attachment and detachment of particles in porous media columns and calculated interparticle forces for platy particles including van der Waals forces, electrical double layer forces, hydration forces and Born repulsion. An interparticle force model was developed using the actual shape of kaolinite particles (hexagonal platelet-like), and it produced results consistent with experimental observations. The force magnitudes followed the decreasing sequence F-F > E-F > E-E, which is the same sequence observed by Ravisangar et al. (2001) in flume erosion experiments for kaolinite. In addition, the pH value observed for the maximum in the percent detachment was around 5, where E-E associations predominate.

2.2 Modes of Erosion

There are three main modes of erosion of fine sediment described in previous research papers. They are surface erosion, mass erosion and fluidization (Mehta 1991). Mehta (1991) believes these different modes "are not wholly distinct and independent of each other, but may be conveniently treated as such".

Surface erosion and mass erosion were documented by Partheniades (1965). The first occurs when particles and small flocs are washed away by hydrodynamic forces, which overcome the bonds formed by interparticle forces. Depending on the sediment structure,

the interparticle forces are either Coulombian or van der Waals force attraction. Surface erosion occurs mainly at low shear stresses not much greater than the critical shear stress of the material, which is the stress at which motion of individual particles or aggregates just begins. On the other hand, mass erosion takes place at shear stresses considerably higher than the critical shear stress, and it happens when the bed fails along a plane such that all the material above the plane is transported. This point of failure was identified by Partheniades (1965) as the macroscopic shear strength of the bed.

Mehta (1991) added a new form of erosion called fluidization, occurring when wave action is followed by entrainment and mixing. Fluidization occurs when water invades the sediment structure and carries the skeletal forces transmitted to the particles. The mud that is formed is entrained by the flowing water to be mixed subsequently with the fluid.

2.3 Erosion Measurement

The most important measures of erosion are the critical shear stress and the erosion rate of the sediment when it is resuspended and transported at higher shear stresses. Different types of experimental equipment have been used to measure erosion properties. These include the linear recirculating flume, rotating anular flume and submerged impinging jet, among other devices. Briaud et al. (1999), developed an apparatus called the erosion function apparatus (EFA), which can test Shelby tube samples by introducing them into a rectangular duct having a cross section 50.8 mm high and 101.6 mm wide. In addition to laboratory measurements, in situ erosion measurements have also been attempted as in

the case of Ravens and Gschwend (1999) who performed measurements of sediment erodibility in Boston Harbor. Still, the most common devices to study sediment erosion phenomena experimentally are the linear recirculating flume and the rotating annular flume.

The linear recirculating flume (Partheniades 1965; McNeil et al. 1996; Dennett et al. 1998; Ravisangar et al. 2001) is basically a straight channel with an open section at the bottom through which a sample of the material is introduced. The flow conditions in the channel are adjusted in order to assure fully developed, uniform, turbulent flow as well as to apply a known shear stress at the bed. A piston is used to extrude the sample into the flume as it is eroded. The height of the material eroded is recorded continuously as well as the time during which it occurs, which when multiplied by the cross sectional area of the sample results in the volumetric or gravimetric, if sediment density is known, erosion rate corresponding to the specified flow conditions. A similar procedure is followed by Briaud et al. (1999), with the difference that the flow through the sample is pressurized.

The other most common device to conduct erosion experiments is the rotating annular flume, (Spork et al. 1995; Mehta and Partheniades 1975, 1982; Mehta et al. 1982; Parchure and Mehta 1985; Mehta 1988; and Zreik et al. 1998). The main difference, other than the fact it employs an annular flume, is in the measure of the erosion. The erosion in the annular rotating flume is measured by monitoring the sediment concentration of the fluid above the eroding surface at given times. However, measures from a Shelby tube or similar can be implemented. The other devices used to measure

sediment erodibility include submerged, turbulent, impinging jets (Mazurek et al. 2001), a water tunnel (Otsubo 1988), and a rotating cylinder (Arulanandan et al. 1975; Ariathurai and Arulanandan 1978; Arulanandan and Perry 1983; Mehta et al. 1982; and Mehta 1991).

In addition to several devices having been used for measuring erosion rates, the criterion for the definition of the critical shear stress is different in some studies. First of all, the three modes of erosion each can have their own critical values of shear stress for initiation of motion. The particle erosion threshold is the first that appears, and it can be visually detected. At higher shear stresses, mass erosion occurs when the macroscopic shear strength of the sediment is exceeded. This can also be visually corroborated. In the same way, a critical shear stress for fluidization occurs at suitable conditions for this type of erosion. On the other hand, some previous studies have focused on the values of the rates of the erosion. For instance, Partheniades (1965), Parchure and Mehta (1985), and Ariathurai and Arulandan (1978) defined the critical shear stress as the intercept with the zero erosion axis of the best fit line of the erosion rate vs. applied shear stress graph. In any case, critical shear stress values for a sediment depend on the sediment, the procedure and apparatus of measurement and the criterion chosen to define the threshold condition.

2.4 Erosion Relationship

Many attempts have been made to relate erodibility to bulk variables of the sediment and pore fluid, and to the conditions of the flow. Among these contributors are McNeil et al. (1996), who made measurements of erosion of undisturbed bottom sediments. Since

erosion properties vary spatially throughout a nonhomogeneous material, they were measured as a function of depth. McNeil et al. (1996) found the most important sediment parameters that affect the erosion phenomenon are the bulk density, water content, average particle size, and organic content. Among the fluid characteristics that affect the erodibility, pH was already mentioned for the results of Ravisangar et al. (2001). It was found that the erosion resistance depends on the bed structure, which in turn is dependent on the pH of the pore water.

Zreik et al. (1998) and Hoepner (2001) attempted to relate erosional behavior to more conventional measures of soil strength. Zreik et al. (1998) compared the erosional and mechanical strength of deposited fine sediment. Mechanical strength was measured in a manner similar to the conventional fall cone, where a cone is released from the sediment surface and penetrates by its own weight for a period of time. Their results showed that erosional strength was one order of magnitude smaller than mechanical strength. Two hypotheses are presented by Zreik et al. (1998): first, the resistance to erosion is governed by the weakest of the individual bonds between flocs, while mechanical resistance is governed by the group of bonds between the flocs available in the sheared sediment mass. Second, for the erosional phenomenon, turbulent eddies in the flow accumulate greater energy that causes sporadic motion of individual flocs before the bulk shear strength of the bed is mobilized. Hoepner (2001) related the stability of fine sediments tested in flume experiments to rheometer measures of yield stress and found that the measured yield stress can be a practical index to predict the erosional strength of undisturbed sediment.

Briaud et al. (2001) using their EFA (Erosion Function Apparatus) measured the erosion rate of fine grained soils, finding that the most common shape of the erosion rate vs. applied shear stress curve is concave up. However, straight and convex shapes were also found. The convex shape was associated with the change of mechanism from surface to mass erosion. Briaud et al. (2001) also correlated the erosion function with soil properties. One of the curve-fitting parameters involved, the critical shear stress, is thought to increase when the soil unit weight, plasticity index, soil shear strength, or fines content increase; and to decrease when the void ratio, soil swell, dispersion ratio, soil temperature or water temperature decrease. However, poor correlations were found with the plasticity index, undrained shear strength, and percent passing the #200 sieve, for example. On the other hand, the initial slope of the erosion rate vs. applied shear stress curve showed an encouraging relationship with the critical shear stress.

The dissimilar approaches to finding a unique relationship for the erosion resistance of sediments is due to the difficulty in characterizing the microstructure from macro properties of the material. This is in particular difficult for fine-grained sediments for which the Shields relationship does not apply. Microstructure properties such as interparticle distance or bed arrangement are not easily converted into particle size distribution and bulk density. In addition, the nonhomogeneity of natural sediments adds more uncertainty in the measured sediment properties. These problems force the use of experimental work to measure soil erodibility although an analytical approach can provide a better understanding of the phenomenon.

2.5 Mathematical Models of Erosion

One of the simplest expressions to quantify the erosion phenomena was developed by Mehta (1991). There are two main components to measure: the rate of sediment mass detached per unit area, known as E or erosion rate, and the excess shear stress (shear stress minus critical shear stress), normalized by the critical shear stress. In this research, these two variables measured from experimental procedures, are linearly related by a constant called M, which depends on the particle and fluid characteristics.

$$E = M \cdot \left(\frac{\tau_b - \tau_c}{\tau_c} \right) \tag{2.14}$$

The last expression is certainly influenced by the definition of the critical shear stress, τ_c. Multiple definitions of τ_c have been used. These include the shear stress below which negligible erosion appears, or the intercept with the zero erosion axis of the best-fit line of the data, or the stress corresponding to a given small value of erosion rate, etc. Regardless of the method used, the M value and the critical stress are unique values for the sediment and fluid conditions present for a given sample, and it is the goal of this research to evaluate experimentally these values for some bridge sites in Georgia to improve bridge scour prediction formulas by including the effect of erodibility for typical river sediments.

Although Equation 2.14 is the most common form to evaluate erosion, there have been several studies that have introduced other variables such as bulk density explicitly into the equation for erosion rate. This is the case of Roberts et al. (1998), who suggested the following equation:

$$E = A \cdot \tau^n \cdot \rho^m \tag{2.15}$$

where A, n and m are constants that depend on the type of sediment. Alternatively, Donat (1929) found that a quadratic relationship would describe better the phenomenon. Donat assumed the following equation:

$$E = b_0 + b_1 \cdot \tau + b_2 \cdot \tau^2 \tag{2.16}$$

where b_0, b_1 and b_2 are experimental constants.

Krone (1999) analyzed experimental results from Roberts et al. (1998) and Zreik et al. (1998). It was concluded that for cases where the only variable is bulk density, erosion rates decrease with increasing bed density. This relationship followed a two-piece linear trend having a breakpoint when the bed structure collapsed due to the mass of soil overburden. See, for example, Figure 2-3 for 14.8 μm silt-size quartz particles from Roberts et al. (1998).

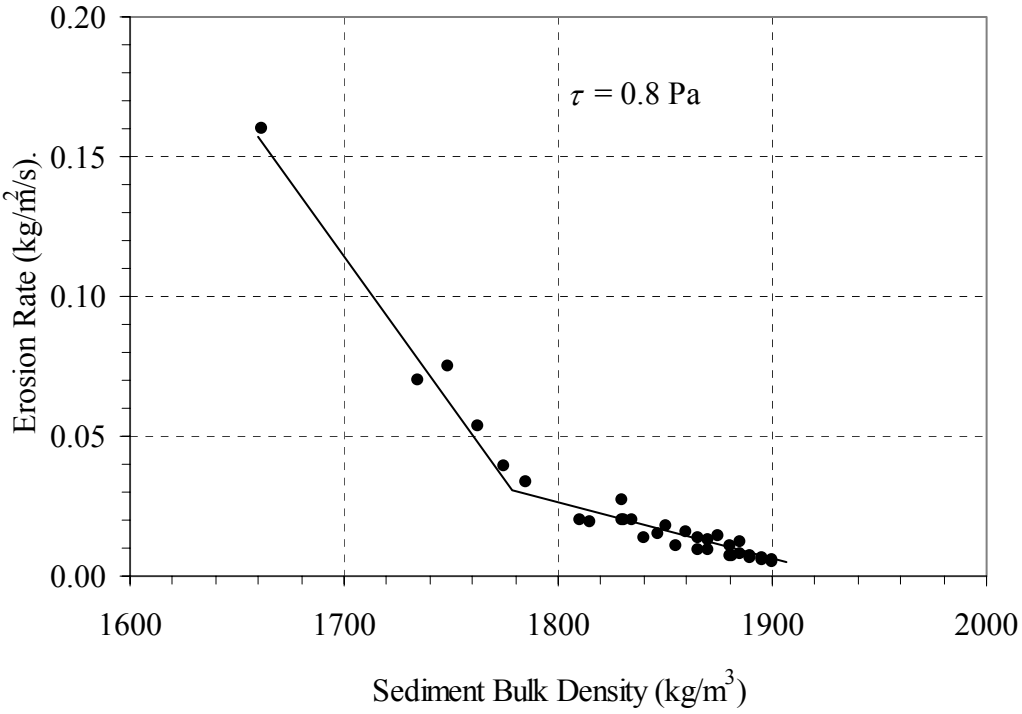

Figure 2-3. Linear erosion rate – bulk density relations at shear stress of 0.8 Pa (Krone 1999).

Lee et al. (1994) summarized measured values for the critical shear stress found by various researchers (Espey 1963, Partheniades 1965, Christensen and Das 1973, Raudkivi and Hutchison 1973, Kandiah 1974, Arulanandan et al. 1973, Arulanandan et al. 1975, Gularte et al. 1977, Fukuda 1978, Thorn and Parsons 1980, Arulanandan 1980, Gularte et al. 1981, Villaret and Paulic 1986, Hwang 1989, and MAST G6M). These values were found using rotating cylinder, straight flume, drill hole, closed conduit, and annular flume apparatuses. The group of samples tested included not only samples created in the laboratory but also included samples taken from the field. The measured values for critical shear stress went up to 61 Pa for a sample with 50 percent of its particles smaller

than 5 microns, and were as low as 0.01 Pa for a loam with 19 percent of its particles smaller than 2 microns and having a sodium adsorption ratio (SAR) equal to 10.7.

Briaud et al. (1999) review some of the values for erosion rate in different materials. The Grand Canyon is taken as an example of erosion in rock giving a value of $4x10^{-9}$ kg/m^2/s. On the other hand, sands can exhibit erosion rates of the order of 4 kg/m^2/s. Clay material will scour at intermediate rates as they corroborated by measurements using the Erosion Function Apparatus (EFA). The range of values found for clay is between 0.0004 and 0.4 kg/m^2/s.

Additional erosion rate relationships, proposed by other investigators, are summarized in Table 2-2 (Mehta 1991).

Table 2-2. Expressions for the rate of erosion of cohesive sediment beds (after Mehta, 1991)

Investigator(s)	Expression	Equation Number
Partheniades (1962)	$E = \alpha_1 \cdot \left[1 - \frac{1}{\sqrt{2\pi}} \int_{-(\beta_1/\tau_b - \beta_2)}^{(\beta_1/\tau_b - \beta_2)} \exp(-\omega^2/2) \cdot d\omega \right]$	(2.17)
Christensen (1965)	$E = \alpha_2 \cdot \left[0.5 - \frac{1}{\sqrt{2\pi}} \int_{0}^{-6.1+(6.18/\sqrt{\beta_3 \tau_b})} \exp(-\omega^2/2) \cdot d\omega \right]$	(2.18)
Kandiah (1974); Arulandan (1975)	$E = \alpha_3 \cdot \left(\frac{\tau_b - \tau_s}{\tau_s} \right)$	(2.19)
Christensen and Das (1973); Raudkivi and Hutchison (1974); Gularte (1978)	$E = \beta_4 \cdot \exp[\alpha_4 \cdot (\tau_b - \tau_s)]$	(2.20)
Lamberton and Lebon (1977)	$E = \alpha_5 \cdot \left(\tau_b^{\beta_s} - \tau_s^{\beta_s} \right) \cdot \tau_b^{1/2}$	(2.21)
Thorn and Parsons (1980)	$E = \alpha_6(z) \cdot [\tau_b - \tau_s(z)]$	(2.22)
Parchure and Mehta (1985)	$E = \alpha_7 \cdot \exp\left[\alpha_8 \left(\frac{\tau_b - \tau_s(z)}{\tau_s(z)} \right)^{1/2} \right]$	(2.23)
Maa and Mehta (1987) (erosion by waves)	$E = \alpha_9 \cdot \left(\frac{\tau_b - \tau_R}{\tau_R} \right)$	(2.24)

CHAPTER III

EXPERIMENTAL MATERIALS AND METHODS

3.1 Sample Characteristics

The Georgia Department of Transportation (GDOT) supplied the sediment core samples tested in this project. The flume experiments were conducted on material collected according to ASTM (D 1587-00): Standard practice for thin-walled tube sampling for geotechnical purposes. In this project, thin-walled tubes were used with a diameter of 76.2 mm (3 in.), length of 910 mm (36 in.) and wall thickness of 1.65 mm (0.065 in.) as shown in Figure 3-1. The crews from GDOT were told the foundation depth of the bridges, and they chose the most convenient drilling method and the sampler insertion method. Boring logs were provided for each of the sites where the samples were extracted. After receiving the samples, they were sealed and stored in a constant temperature room vertically confined inside a wooden box, until the soil and flume tests were ready to begin. Some minor leaking of water through the bottom of the tube was observed in a few cases. However, none of the samples appeared to have their surface dried out.

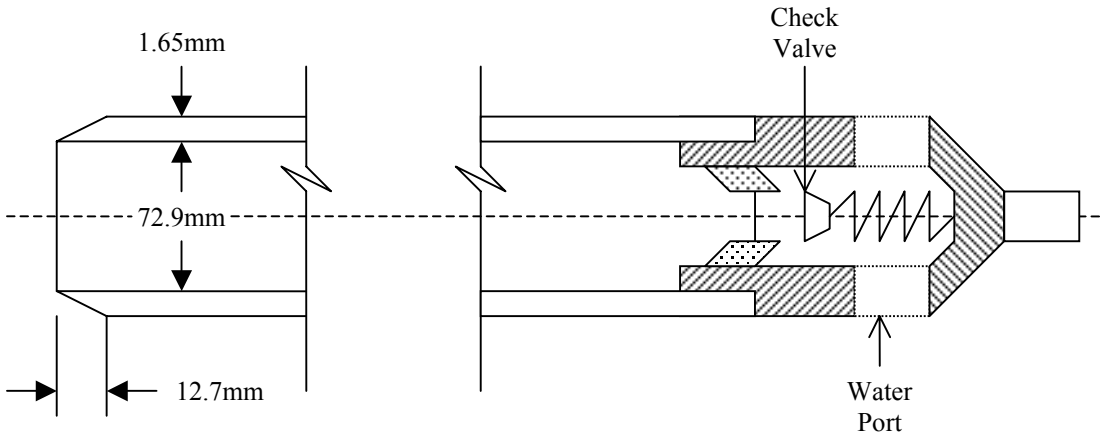

Figure 3-1. Undisturbed 3-inch thin walled sampler (Sowers 1979).

Ten bridge sites in the state of Georgia were chosen for collection of samples from their foundations on which to perform flume tests and measure soil characteristics. Flume tests were executed with the objective of finding the particular critical shear stress and erosion rate constant at the respective site. A number of soil properties were measured including size distribution, water content, bulk density, organic matter, and liquid and plastic limit for the fine-grained samples. These sites were geographically distributed in such a way that they fell into different river basins and into different physiographic regions.

Four main regions can be roughly identified in Georgia. They are the Valley and Ridge, the Blue Ridge, the Piedmont and the Coastal Plain regions. Samples were collected from each of these regions. Figure 3-2 shows the location of the sites, and Table 3-1 provides further information on the bridge locations and the physiographic regions in which they are found.

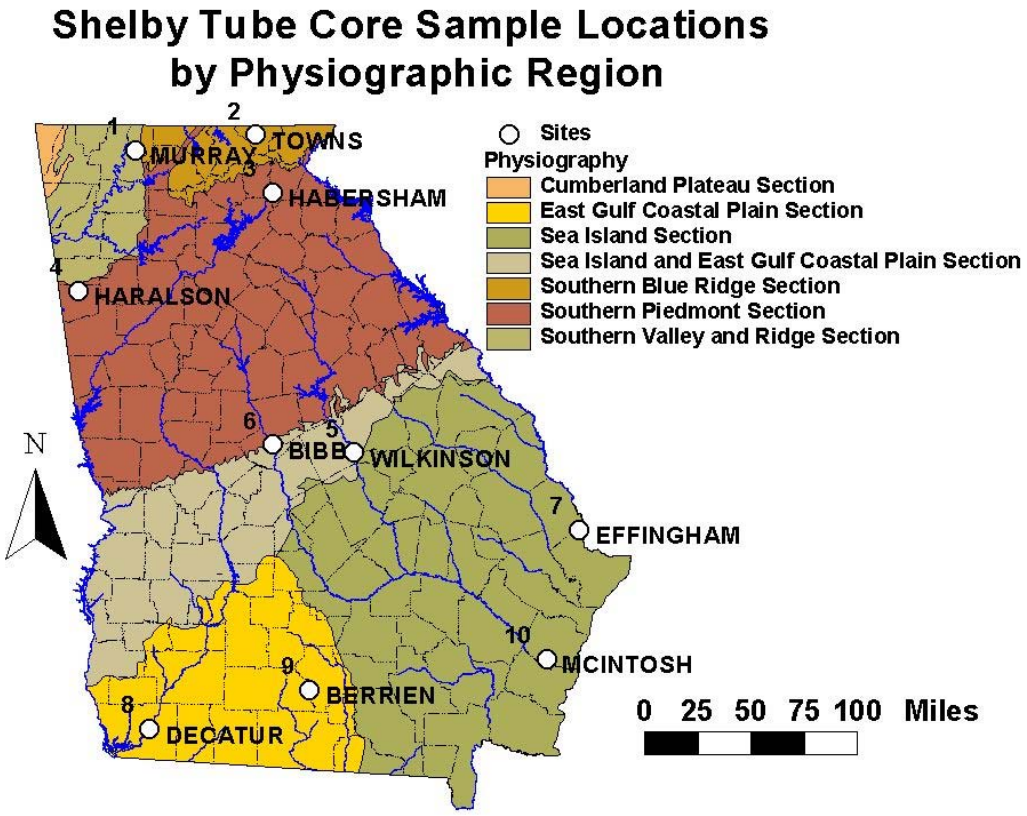

Figure 3-2. Shelby tube core sample locations (Digital Environmental Atlas of Georgia, Alhadeff et al. 2000).

Table 3-1. Location of samples and description of physiographic regions.

	County	Location	Physiographic Section	Major Land Resource Area	Latitude and Longitude
1	Murray	US 411 over Mill Creek	Southern Valley and Ridge Section	Southern Appalachian	34.8189º, 84.7647º
2	Towns	SR 288 over Fodder Creek	Southern Blue Ridge Section	Blue Ridge	34.9275º, 83.7625º
3	Habersham	Duncan Bridge Rd over Chattahoochee River	Southern Piedmont Section	Southern Piedmont	34.5406º, 83.6228º
4	Haralson	US 27 over Tallapoosa River	Southern Piedmont Section	Southern Piedmont	33.8642º, 85.2097º
5	Wilkinson	SR 57 over Oconee River	Sea Island and East Gulf Coastal Plain Section	Southern Coastal Plain	32.7817º, 82.9586º
6	Bibb	US 80 / 5th St over Ocmulgee	Southern Piedmont Section	Sand Hill	32.8380º, 83.6212º
7	Effingham	I-95 (NBL) over Savannah River	Sea Island Section	Atlantic Coast Flatwoods	32.2351º, 81.1540º
8	Decatur	SR 1b / Calhoun St over Flint River	East Gulf Coastal Plain Section	Southern Coastal Plain	30.9061º, 84.5886º
9	Berrien	SR 76 over Withlacoochee River	East Gulf Coastal Plain Section	Southern Coastal Plain	31.1769º, 83.3225º
10	McIntosh	US 17 over Darien River	Sea Island Section	Atlantic Coast Flatwoods	31.3675º, 81.4364º

In addition to the material collected from the ten sites, two samples were prepared to calibrate the erosion measurements and to provide reference measurements on coarse sediments. The first was bed material collected from Peachtree creek inside the Atlanta metro area with low clay content. The second reference material tested was a pure commercial sand with a median size of 1.16 mm without any silt and clay content having a coefficient of uniformity of 1.5, which is the ratio of the diameter of the particles corresponding to 60% and 10% finer on the cumulative particle-size distribution curve.

3.2 Experimental Setup

A rectangular, tilting, recirculating flume located in the hydraulics laboratory at the Georgia Institute of Technology was utilized to erode the core samples. The flow in the flume can be driven by either of two variable-speed pumps for low or high flows. Figure 3-3 shows the flume. It measures 6.1 m (20 ft) long, 0.38 m (1.25 ft) wide and a maximum of 0.38 m (1.25 ft) deep. The flume bed has fixed small gravel (d_{50} = 3.3 mm) to assure fully-developed and fully-rough turbulent flow. At the end of the flume there is a holding tank with a volume of 1.9 m^3, which feeds both pumps. Only one pump is operated at a time. A 0.15 m (6 in.) pipe circulates the flow from the large pump to the head box of the flume, which contains an elliptical wall transition and flow stilling devices. In the same way, on the other side of the flume, a 0.10 m (4 in.) pipe feeds water from the small pump into the head box. The small pump is a progressing cavity pump for slurries while the large pump is a low-speed, large-impeller centrifugal pump designed for solids pumping.

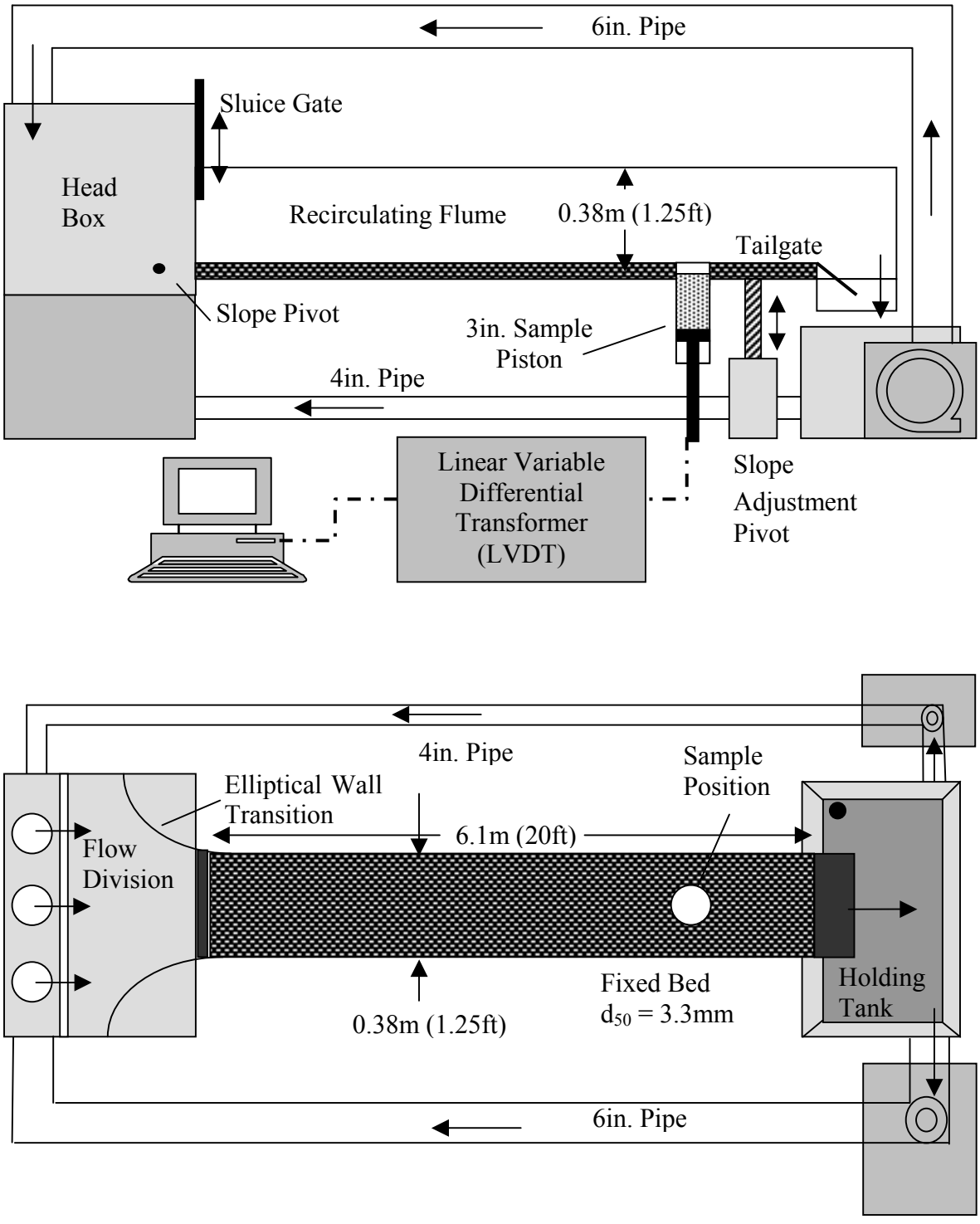

Figure 3-3. Recirculating flume for erosion testing.

The operating variables of the flume are discharge, slope and flow depth. The flow rate is adjusted based on the rotational speed at which the pump is operating. Flow calibration tables were developed by previous researchers (Ravisangar 2001 and Hoepner 2001). The 4 in. pump has a working range from 3.4 L/s to 14.7 L/s (0.12 – 0.52 cfs). The 6 in. pump has a working range from 14.2 L/s to 70.8 L/s (0.50 – 2.5 cfs). Figures 3-4 and 3-5 show the regression analysis performed to calibrate the pump flow rate. The small pump is calibrated with respect to the frequency of rotation and the large pump is calibrated using a bend meter with flow rate measured using a weighing tank as a function of the bend-meter manometer deflection.

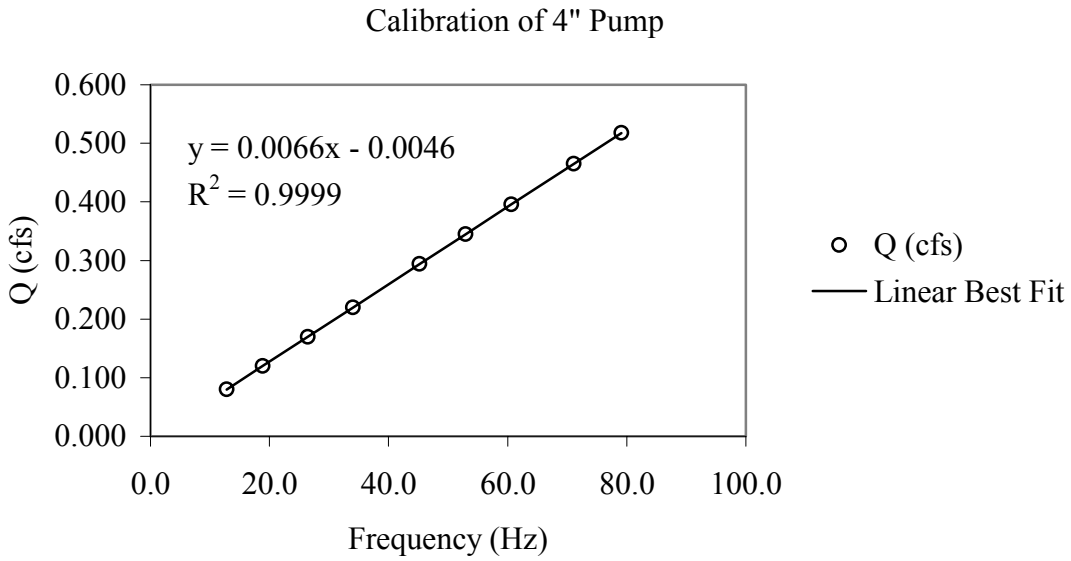

Figure 3-4. Calibration of 4 in. pump.

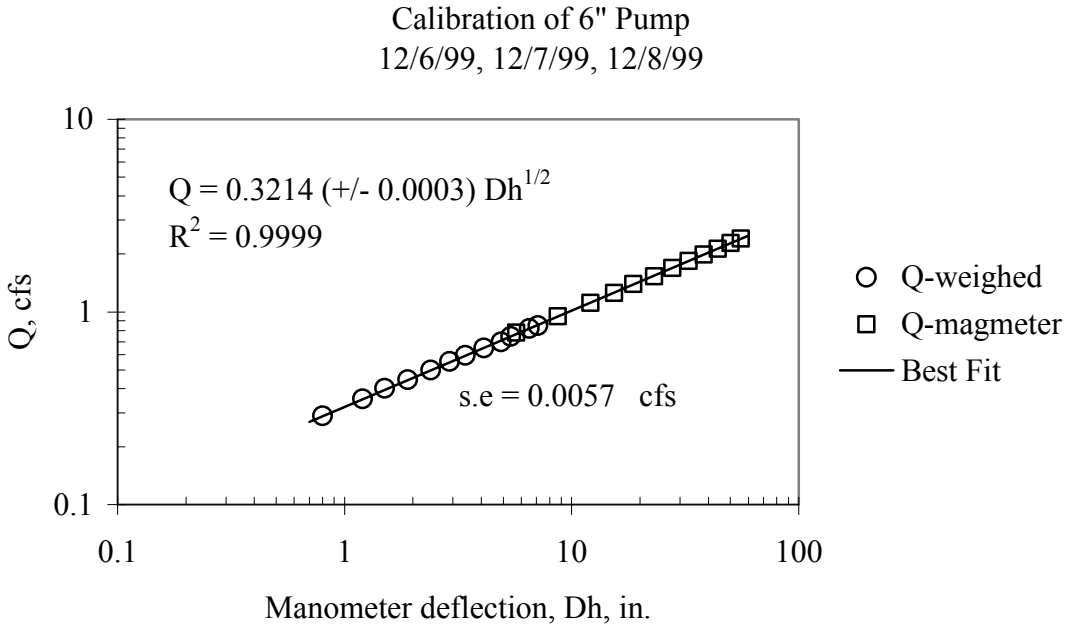

Figure 3-5. Calibration of 6 in. pump bend meter.

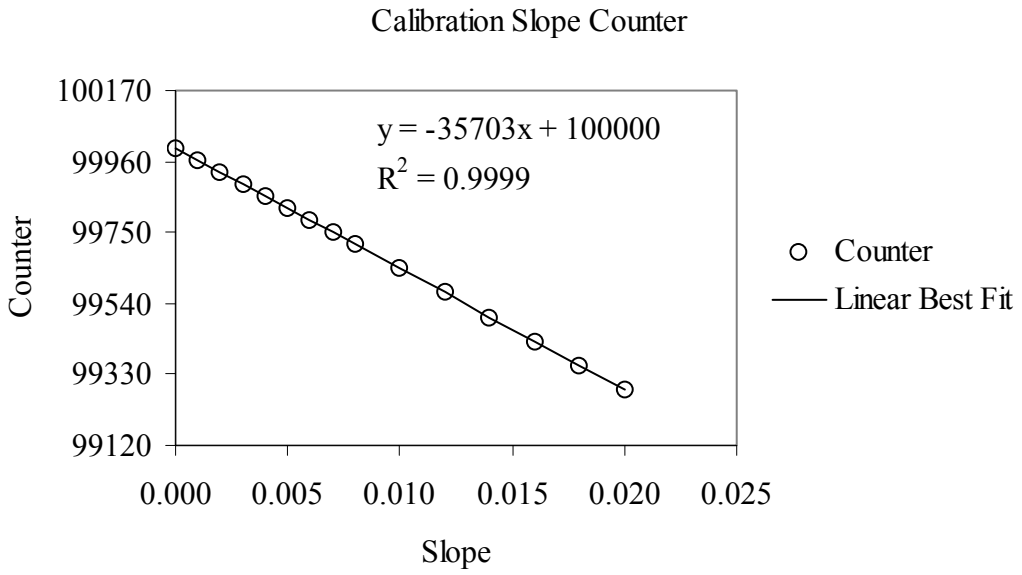

Figure 3-6. Flume slope calibration.

The tilting flume can be set at slopes between 0 and 0.02 m/m. Although the flume can be tilted to reach steeper slopes, unstable flows will predominate beyond this slope value. The slope is measured by a slope counter, which counts the revolutions of the gear mechanism that raises and lowers the flume. Figure 3-6 shows the slope calibration.

The flow depth is set using either the tailgate for subcritical cases or the upstream sluice gate for supercritical flow. The values of the normal depth are found in an initial set of experiments using the asymptotic approach depth of gradually-varied flows. The depths used are normal because that guarantees a uniform flow and the simplifications that this implies. For example, the applied shear stress (τ_0) at the flume centerline where the sediment sample is located can be found by multiplying the water specific weight (γ_w), the flow depth (y), and the slope (S) for a given flow situation, as given by

$$\tau_0 = \gamma_w \cdot y \cdot S \tag{3.1}$$

This expression was corroborated by Ravisangar (2001) by comparing the shear stress calculated from it with the applied shear stress determined from the slope of the velocity profile measured at the flume centerline using a laser Doppler velocimeter (LDV).

The bed shear stresses ranged from 0.4 Pa to 21 Pa. The 4-in. pump produces flow rates up to 14.7 L/s (0.52 cfs) resulting in a maximum shear stress of approximately 3 Pa. The 6-in pump setup can reach discharges of 70 L/s (2.5 cfs) and shear stresses up to 21 Pa.

The range of flow depths used in this rectangular flume is from 0.04 m to 0.2 m. The maximum average velocity achieved in the flume was approximately 1.7 m/s.

For each experiment run, uniform flow depths were set with the tailgate or sluice gate based on the initial measurements of normal depth and the corresponding roughness coefficient for each combination of flow rate and slope. These depths were verified at the test section and along the flume. To ensure accurate uniform flow depths, it was necessary to maintain the Froude number (**F)** below 2 in order to avoid roll waves, and to apply the sidewall correction to account for the smooth walls for different values of the Reynolds number (**Re**). The Froude number is defined by

$$\mathbf{F} = \frac{V}{\sqrt{g \cdot y}} \tag{3.2}$$

Also the Reynolds number (**Re**) and friction factor (*f*) were calculated and defined by

$$\mathbf{Re} = \frac{4 \cdot R \cdot V}{\nu} \tag{3.3}$$

$$f = \frac{8 \cdot \left(\gamma_w \cdot R \cdot S\right)}{\rho \cdot V^2} \tag{3.4}$$

in which R = hydraulic radius; V = mean velocity; ν = kinematic viscosity of the water; γ_w = water specific weight; S = slope; and ρ = water density.

Because the flume walls are smooth, while the bed is rough, the side-wall correction procedure described by Julien (1995) and included in Hoepner (2001) for this same flume was applied to determine the wall friction factor, f_w; bed friction factor, f_b; bed hydraulic radius, R_b; and Manning's roughness coefficient for the bed, n_b , calculated from the bed friction factor:

$$f_w = 0.0026 \cdot \left[Log\left(\frac{\mathbf{Re}}{f} \right) \right]^2 - 0.0428 \cdot Log\left(\frac{\mathbf{Re}}{f} \right) + 0.1884 \tag{3.5}$$

$$f_b = f + \frac{2 \cdot y}{b} \cdot \left(f - f_w \right) \tag{3.6}$$

For a given uniform flow condition, the overall friction factor is obtained from the Darcy-Weisbach equation by substituting the measured slope, hydraulic radius, and mean velocity as

$$f = \frac{8gRS}{V^2} \tag{3.7}$$

Values of f_w and f_b follow from (3.5) and (3.6). Then the bed hydraulic radius R_b is calculated as

$$R_b = \frac{f_b}{f} \cdot R \tag{3.8}$$

Finally, the relationship between Manning's n and the friction factor f is utilized to obtain the Manning's roughness coefficient for the bed alone, n_b:

$$n_b = \frac{K_n}{(8g)^{1/2}} \cdot f_b^{1/2} \cdot R_b^{1/6} \tag{3.9}$$

In addition to the Manning's roughness coefficient of the bed, n_b, Ravisangar (2001) determined the equivalent sand-grain roughness of the flume, k_s, using a nonlinear regression of Keulegan's equation:

$$\frac{n_b}{k_s^{1/6}} = \frac{\frac{K_n}{(8g)^{1/2}} \cdot \left(\frac{R_b}{k_s}\right)^{1/6}}{2.0 \cdot Log\left(12.2 \cdot \frac{R_b}{k_s}\right)} \tag{3.10}$$

The known variables are n_b and R_b, and the value of k_s is chosen as the value that produces the best fit of Equation 3.10 to the data. The result is

$$k_s = 0.0181(+/-0.00083)\ ft$$
or
$$k_s = 5.52(+/-0.25)\ mm$$

The best-fit value is related to the median bed sediment size by $k_s = 1.67 d_{50,}$ and the plot of $n_b/k_s^{1/6}$ as a function of R_b/k_s is shown in Figure 3-7. This result is used to calculate the normal depths for additional shear stress conditions using Manning's equation. The

calculated shear stress conditions range from 13 Pa to 21 Pa and should follow the same Keulegan's equation fit. These predicted normal depths were corroborated in the flume experiments.

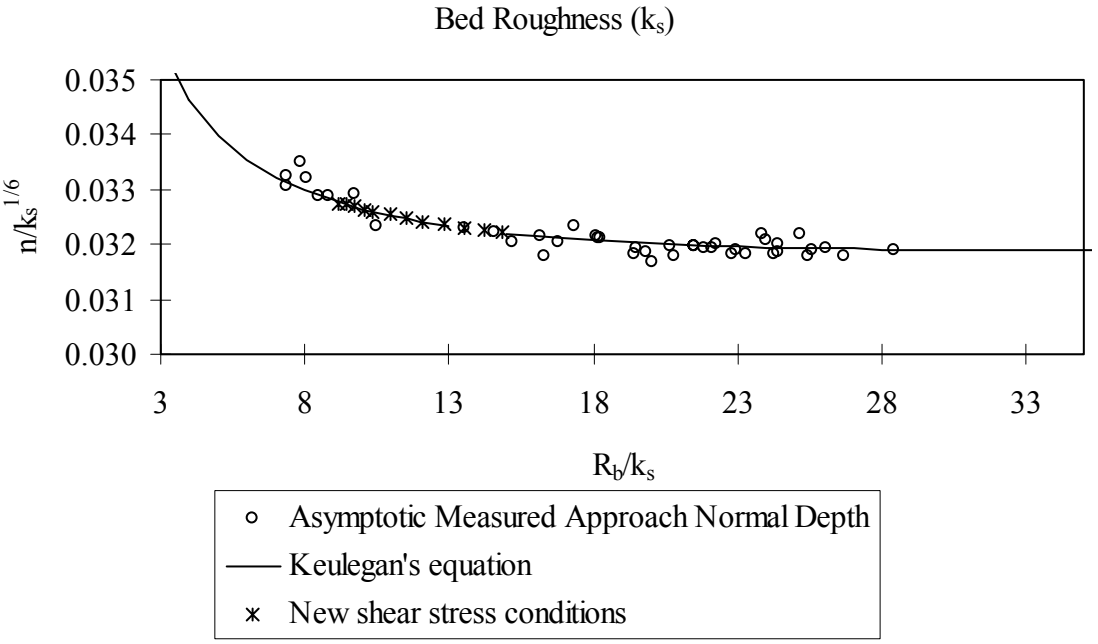

Figure 3-7. Measured and calculated bed roughnesses for new shear stress conditions.

Once the Shelby tube is placed below a circular opening in the bottom of the flume, the measurement of the erosion of the material is performed with a linear variable differential transformer (LVDT) as the material is pushed manually upwards by a hydraulic jack through the bottom of the channel (see Figure 3-3). A computer program was written in Visual Basic to read and record the displacement of the material. The LVDT was calibrated to find the displacement-voltage relationship as shown in Figure 3-8.

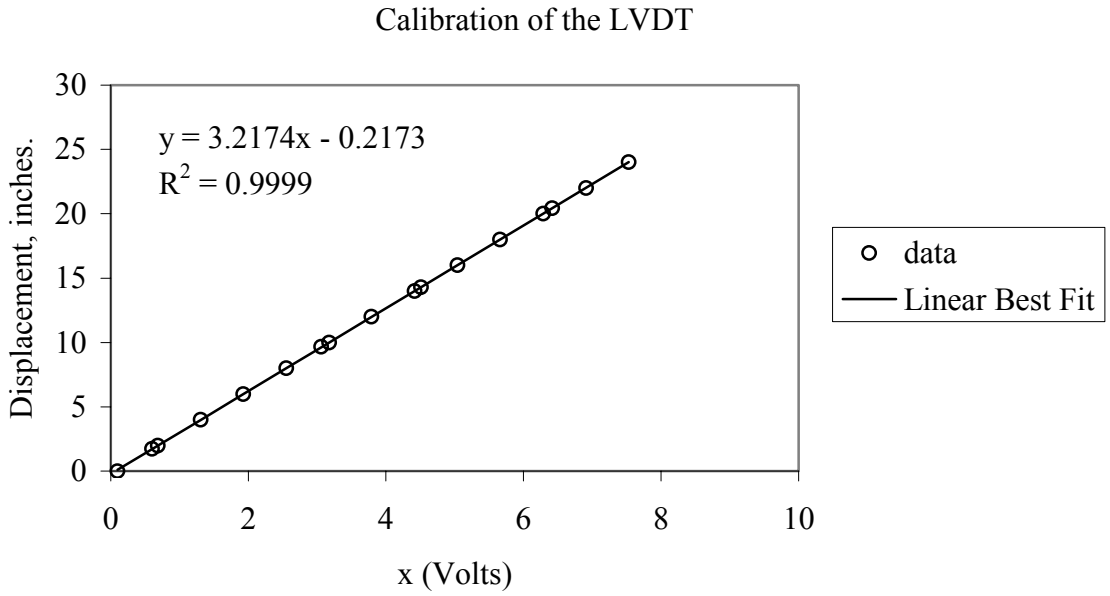

Figure 3-8. Calibration of the LVDT to determine piston displacement.

3.3 Method to Obtain Critical Shear Stress and Erosion Rate

The observed erosion fell mainly in two of the three modes of erosion identified by Mehta (1991). At low shear stresses, just above the critical shear stress, single particles were dislodged over the entire bed, which is identified as surface erosion. The other type of erosion observed in this study was mass erosion, which occurred at shear stress values greater than those that created surface erosion. In this last case, the material failed along a plane, transporting all the material above it. Even though these two mechanisms could be distinguished, there was not a clear line of demarcation between them. These two mechanisms usually coexist but the predominance of one over the other is likely to depend on the amount of fine material present in the sediment and the size of the fine material.

The experimental setup is based on visual observation of the sample while eroding. As the material is eroded over the exposed area of the Shelby tube sample, which is a circle approximately 7.5 cm (3 in.) in diameter, the operator pushes the sample upward with the piston, maintaining the sediment surface level with the top of the gravel bed of the rectangular flume. The material eroded is recorded as the mass per unit area removed in units of kg/m^2 based on piston displacement and the dry density of the sample. This erosion is produced in a measured interval of time. These two variables, material eroded and time, are plotted against each other and linear regression is applied to find the erosion rate at the flow condition for which it is measured. As long as material is available in the Shelby tube, a single-condition test can be repeated to account for operator effects. For the uniform sand test, in which unlimited material was available, a second series of

erosion tests was performed resulting in approximately 12% difference in the erosion rate values.

Figure 3-9 shows a typical measurement of piston displacement, tracked by the LVDT, vs. time. This example case is sand with a median size of 1.16 mm which is being eroded under an applied flow shear stress of 3.5 Pa.

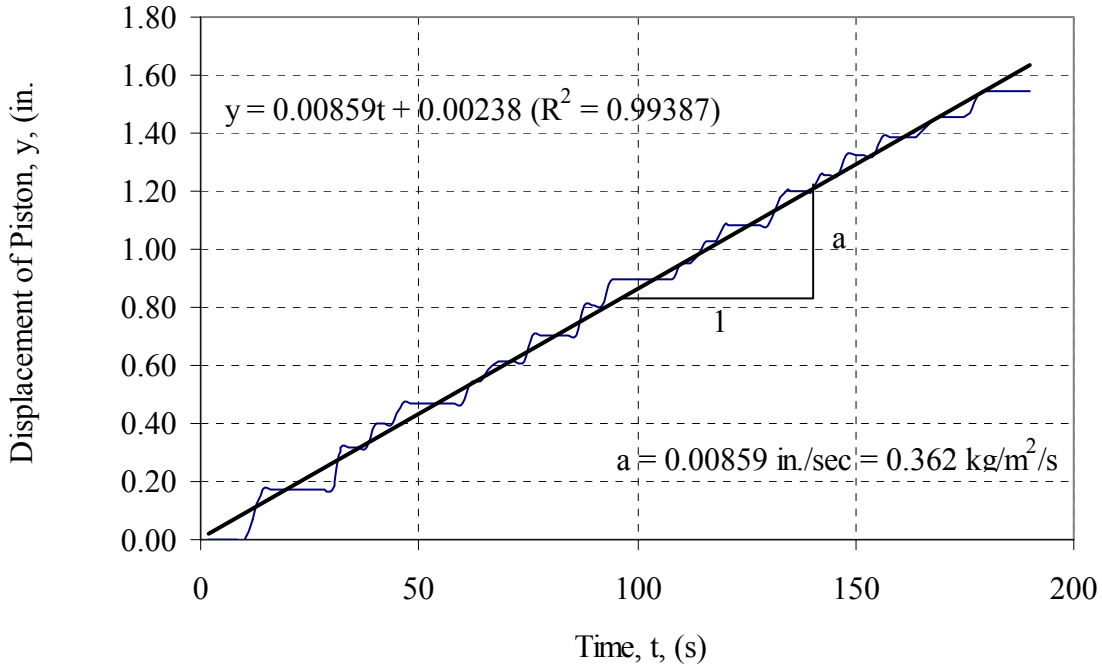

Figure 3-9. Example flume erosion rate measurement, sand d_{50} = 1.16mm, applied shear stress = 3.53 Pa

In order to convert from vertical displacement of the sample to mass eroded, the following calculation is made

$$Mass\ eroded\ \ per\ unit\ surface\ area = \frac{Area \cdot \Delta y \cdot \rho_{dry}}{Area} = \Delta y \cdot \rho_{dry} \tag{3.11}$$

in which *Area* = cross sectional area of the Shelby tube; *Δy* = vertical displacement of the sediment; and ρ_{dry} = dry density of the sediment. Then, the erosion rate is given by

$$E = Erosion\ Rate = \frac{\Delta y \cdot \rho_{dry}}{\Delta t} \tag{3.12}$$

where *Δt* = time interval over which the erosion occurs, and *Δy/Δt* is the slope of the best fit line of the electronically recorded piston displacement vs. time data, as shown in Figure 3-9, for a given applied shear stress.

Another experimental issue that had to be addressed was the suspended sediment load transported in the recirculating flume. This load increased as the experiment progressed due to the recirculating water, and in some cases the suspended sediment concentration reached a point that affected the visibility of the top of the sediment sample and the accuracy of the measurement. In these cases, the water in the system was changed, and the eroded material was removed from the tail tank. Then the experiment was continued for additional shear stress values. This added several hours to the experimental test procedure.

For a given sediment sample, it is expected that for a specific flow condition (bed shear stress), a particular value of erosion rate will be produced. Thus, once the critical shear

stress is found, a series of increasing shear stresses can be applied to measure the erosion rate for each one. Given the heterogeneity of natural sediments, slightly different erosion rates may occur for the same flow condition, but when large differences are observed in the erosion rate values, there is evidence of a change in the type of sediment due to sediment stratification. These abrupt changes in erodibility occurred in nearly all of the samples. When the changes were detected, the process of finding the critical shear stress was started again, and sediment property tests were made on the new sediment layer.

Calculating Critical Shear Stress and Erosion Rate

For the given experimental setup for measuring erosion of Shelby tube samples, there is a limiting minimum erosion rate that can be measured. The most important parameter to determine is the critical shear stress, which depends on the measured erosion rates at different values of shear stress. In this study, the minimum measured erosion rate depends on the uncertainty in the observed top of the sediment sample during erosion and the length of the erosion test. Running a single flow condition at a particular shear stress for 3 hours, for example, could result in measured erosion rates as small as 0.001 $kg/m^2/s$. McNeil et al. (1996), who performed erosion measurements using a similar straight rectangular flume, defined their minimum erosion rate to be less than 0.1 cm of sediment eroded in 15 minutes, which is of the same order as in this experimental setup.

In order to avoid any subjectivity in the definition of the critical shear stress, the best two models explored in this study, which produced a good fit for the measured data of erosion rate vs. shear stress, are defined in such a way that they produce the minimum difference

in critical shear stress values. Three basic relationships (linear, exponential and power) were tried in this study. The best two models, with respect to goodness of fit and minimum standard error of erosion parameters, are linear and exponential with the following equations:

Linear model (or piecewise linear),

$$E = M \cdot \left(\frac{\tau - \tau_c}{\tau_c} \right) \tag{3.13}$$

in which E = erosion rate; M = erosion rate constant; τ_c = critical shear stress.

Exponential model,

$$E = E_c \cdot e^{a \cdot \left(\frac{\tau - \tau_c}{\tau_c} \right)} \tag{3.14}$$

in which E_c = critical erosion rate; a = erosion rate constant; τ_c = critical shear stress.

The defined critical shear stress for the linear model is the extrapolation of the best-fit line for erosion vs. applied shear stress to the erosion rate equal to zero. Flow conditions under this critical value of shear stress produce insignificant erosion. In the exponential model, a value of negligible erosion rate has to be specified in order to find the intercept and thus the critical shear stress, given that it is an asymptotic model. The critical erosion

rate is defined in this study as the value of erosion rate that gives a minimum least squares error between the critical shear stress values found by linear regression and by exponential regression. This value of the erosion rate was found to be 0.00190 kg/m^2/s. This procedure is applied to a reference sediment as illustrated and described in more detail in the following paragraph.

Two materials were used to calibrate the experimental setup and to provide a reference for coarse sediments. The first material was uniform sand with a median size of 1.16 mm and coefficient of uniformity of 1.5, which is the ratio of the diameter of the particles corresponding to 60% and 10% finer on the cumulative particle-size distribution curve. The second was a core sample from the bed of Peachtree Creek in the Atlanta metro area that was mostly sand, but with five percent of fine material (clay and silt).

Figure 3-9 includes a comparison of the two models that were found to be better fits. The first one is a piecewise linear model with a critical shear stress of 1.0 Pa. This critical shear stress is found by extrapolating the first part of the best-fit straight line to intercept with the shear stress axis. The second model is an exponential model that results in a critical shear stress of 0.38 Pa when it is extrapolated to intercept the value assumed as critical erosion rate (0.00190 kg/m^2/s). The values obtained from Shields' diagram range between 0.62 and 0.88 Pa which compares favorably with the linear model as shown in Figure 3-10, particularly since the data point with the smallest measured erosion rate falls within the Shields interval. In addition, the measured erosion rates are compared with

calculated erosion rates using Karim's sediment transport formula for sand transport in rivers given by (Sturm 2001)

$$\frac{q_t}{\sqrt{(SG-1)\cdot g\cdot d_{50}^3}} = 0.00139\cdot\left(\frac{V}{\sqrt{(SG-1)\cdot g\cdot d_{50}}}\right)^{2.97}\cdot\left(\frac{u_*}{w_f}\right)^{1.47} \tag{3.15}$$

in which q_t = total volumetric sediment discharge per unit width; SG = specific gravity; d_{50} = median size; V = flow velocity; u_* = shear velocity; and w_f = fall velocity. Although there is agreement of Equation 3.15 with the data at the lower erosion rates, there are some discrepancies at higher erosion rates. This is thought to be the result of bed forms being absent in the flume test because of the small size of the sample, but their effect is included in the data on which Equation 3.15 is based. A flat bed is predicted for the lower shear stresses in the flume while bed forms would be expected at the higher shear stresses.

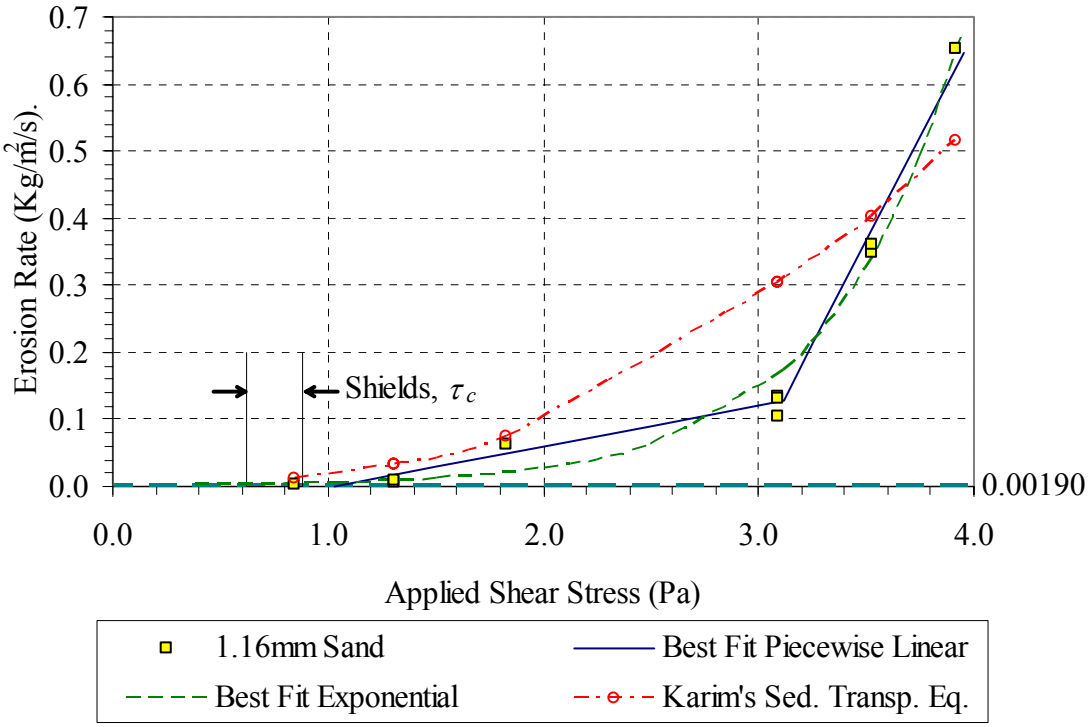

Figure 3-10. Erosion rate vs. applied shear stress data and curve fits for uniform sand d_{50} = 1.16 mm compared to the calculated erosion rates using Karim's sediment transport formula, and also showing Shields critical shear stress values.

Figure 3-11 shows the results of the erosion tests performed on a material with some content of fine particles from Peachtree Creek. In this case, the critical shear stress found via extrapolation of its linear regression (2.18 Pa) is considerably higher than the Shields diagram value (approximately 0.18 Pa). Also, the calculated erosion rates using Karim's sediment transport formula (Equation 3.15) for pure sand are several times higher than observed in the lab. These results show a likely dependency of the erosion characteristics of the sediment on its fine material content. Fine material gives it additional strength to resist erosion.

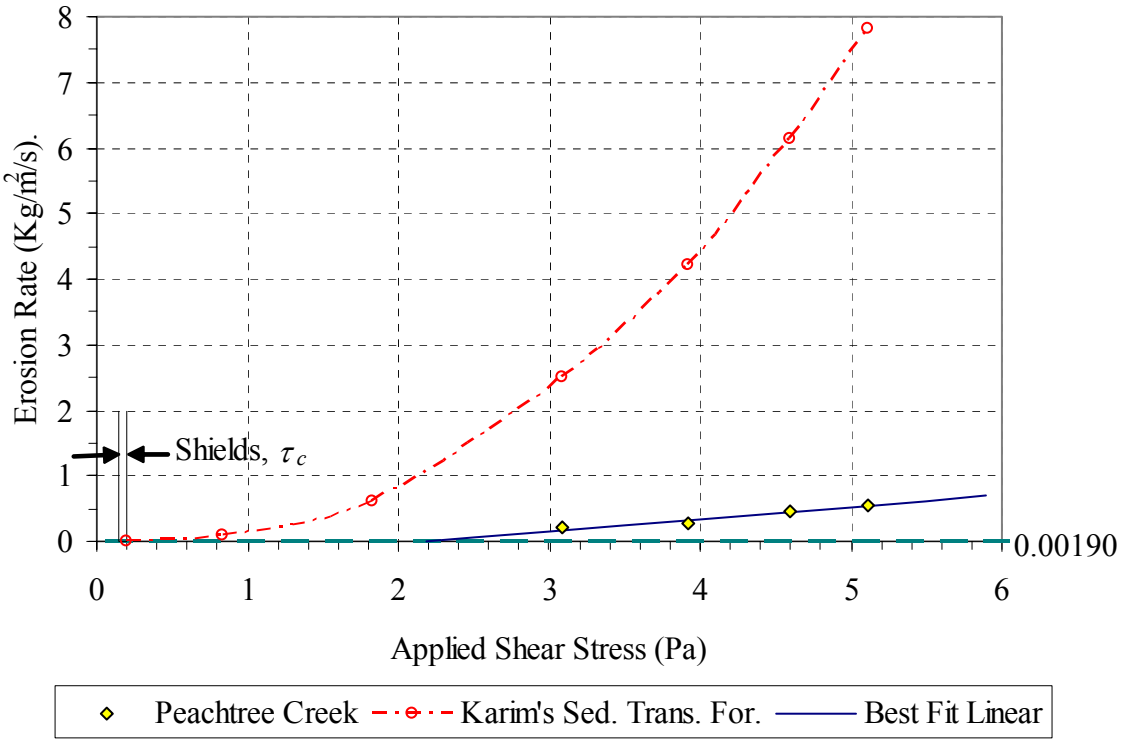

Figure 3-11. Measured erosion rate vs. applied shear stress for bed material from Peachtree Creek with 5% fines compared to the calculated erosion rates using Karim's sediment transport formula and also showing Shields critical shear stress values.

Table 3-2 gives detailed information about the materials used to evaluate the experimental setup. Although the sample from Peachtree Creek consists of only 3 percent silt and 2 percent clay, this is clearly sufficient to provide significant interparticle forces.

Table 3-2. Results of erosion tests and soil property tests on pure sand and a bank sample from the North Fork Peachtree Creek.

Site	Sand d50=1.16mm	Peachtree Creek
Critical Shear Stress (Pa)	1.03	2.18
Sediment	SP	SP
Group Name	Poorly Graded Sand	Poorly Graded Sand
Color	Gray Brown	Gray
Dry Density (Kg/m^3)	*1658*	*1360*
e (void ratio)	*0.60*	*0.95*
Bulk Density (Kg/m^3)	*2025*	*1799*
Water Content	*22%*	*32%*
Specific Gravity	*2.65*	*2.65*
Organic Matter	*0.0%*	*0.0%*
Liquid Limit	*NP*	*NP*
Plasticity Index	*NP*	*NP*
d_{50} (mm)	*1.16*	*0.21*
Sand	*100%*	*95%*
Silt	*0%*	*3%*
Clay	*0%*	*2%*

3.4 Soil Characteristics Testing

Conventional soil tests were performed on the material recovered from the top and the bottom of the Shelby tube or wherever there was a change in material properties. A change of material could be perceived visually or when the erosion rates changed drastically. The soil tests included the following: dry density, water content, specific gravity, organic matter content, liquid limit and plasticity index, sieve analysis and hydrometer test to find the size distribution of the Shelby tube samples. Because of the natural source of the soil material, heterogeneity of the samples was expected and found in several cases.

Two methods were used to estimate the dry density of the material. The first procedure consisted in extruding a representative height of the sample, approximately 0.05 m (2 in.), with the exact height of the sample measured using the LVDT. The other method was to cut a piece of tube with the sample fully filling it, and measure the dimensions of the cylinder with a caliper. The soil was dried and weighed, and the dry density (ρ_{dry}) was determined from

$$\rho_{dry} = \frac{M_s}{V_T} \tag{3.16}$$

in which M_s = mass of soil particles; V_T = total volume of soil particles and voids.

The water content was calculated following the directions of ASTM D 2216-98: Standard test method for laboratory determination of water (moisture) content of soil and rock by mass. This procedure defines the water content by

$$WC = \frac{M_{cws} - M_{cs}}{M_{cs} - M_c} = \frac{M_w}{M_s} \tag{3.17}$$

where WC = water content; M_{cws} = mass of container and wet specimen; M_{cs} = mass of container and oven dry specimen; M_c = mass of container; M_w = mass of water; and M_s = mass of soil particles.

The bulk density, ρ_{bulk}, is defined by

$$\rho_{bulk} = \frac{M_s + M_w}{V} = (1 + WC) \cdot \rho_{dry} \tag{3.18}$$

The void ratio, e, is defined as the volumetric ratio of voids (water and air) to solids and is given by

$$e = \frac{V_T - V_s}{V_s} = \frac{\rho_s}{\rho_{dry}} - 1 \tag{3.19}$$

in which V_T = the total volume of the soil sample, V_s = the volume of the soil solids, ρ_s = the density of the soil solids, and ρ_{dry} = dry density.

The specific gravity was found following the procedure of ASTM D 854-00: Standard test methods for measuring specific gravity of soil solids by water pycnometer. This standard describes the apparatus and materials needed to find the specific gravity defined by

$$SG = \frac{\rho_s}{\rho_w} = \frac{M_s}{M_{\rho w} - \left(M_{\rho ws} - M_s\right)} \tag{3.20}$$

in which ρ_s = the density of the soil solids; ρ_w = the density of water; M_s = the mass of the oven dried soil solids; $M_{\rho w}$ = the mass of pycnometer and water; and $M_{\rho ws}$ = the mass of pycnometer, water, and soil solids.

In order to carry out the organic matter test, one of the environmental engineering laboratories in the School of Civil and Environmental Engineering at Georgia Tech provided an oven that reaches 500°C (932°F). ASTM D 2974-00: Standard test method for moisture, ash, and organic matter of peat and other organic soils describes the process used. The organic matter content is defined by

$$OM = \frac{M_s - M_{ash}}{M_s} \tag{3.21}$$

where M_s = the mass of the oven dry soil solids; M_{ash} = the mass of the soil after being in the oven at 440°C (824°F).

The plasticity of a soil is indicative of the particle size and its clay content. The ASTM D 4318-00: Standard test methods for liquid limit and plasticity index of soils gives the

guidelines to obtain the plasticity chart, as shown in Figure 3-12, and classify fine-grained soils having a high content of fine material.

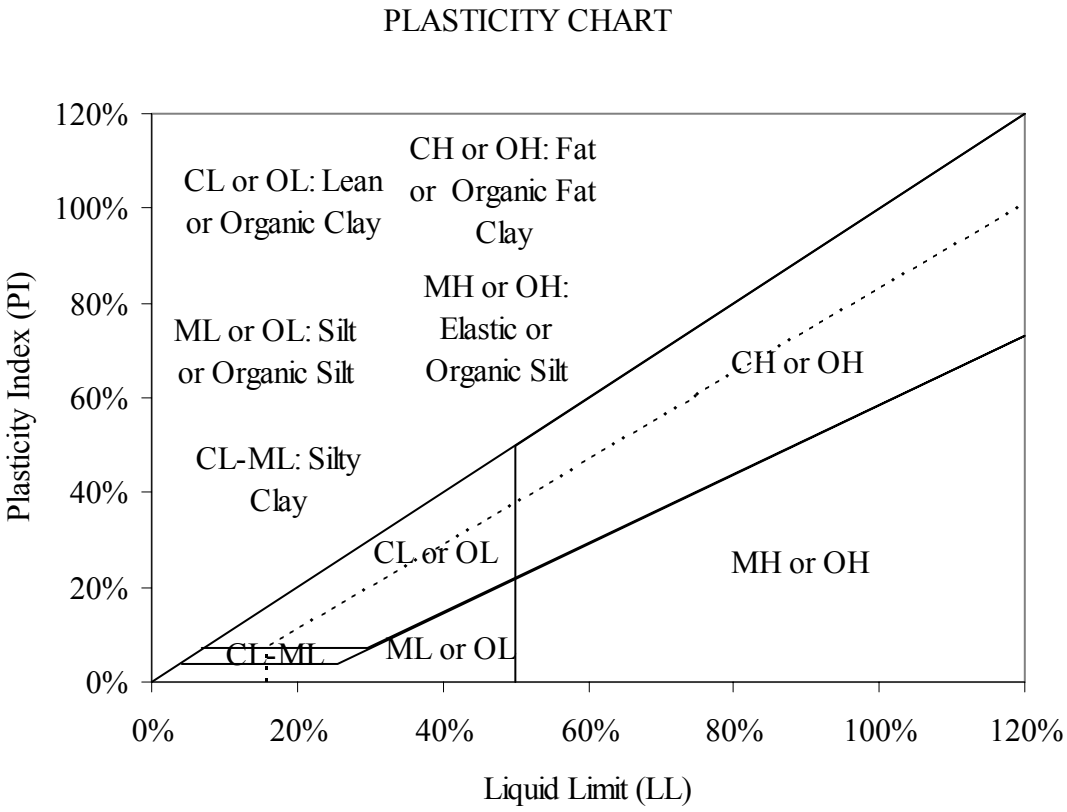

Figure 3-12. Soil plasticity chart.

Size distribution is found by performing a sieve analysis and a hydrometer test according to the guidelines of ASTM C 136-01: Standard test method for sieve analysis of fine and coarse aggregates, and ASTM D 422-63 (reapproved 1998): Standard test method for particle-size analysis of soils. Figure 3-13 shows a typical size distribution plots for several samples.

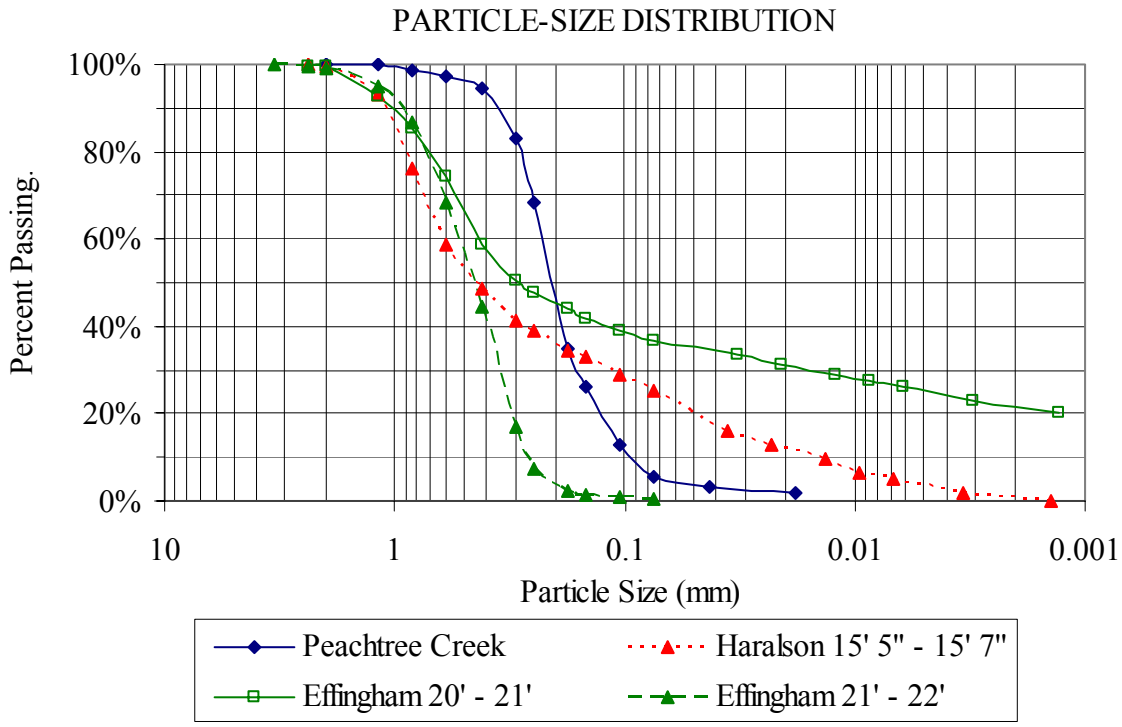

Figure 3-13. Typical particle size distribution.

CHAPTER IV

RESULTS AND ANALYSIS

4.1 Sediment Properties and Geographic Setting

The state of Georgia can be divided into four main physiographic regions based on its geologic formation, as described previously in Chapter III. The Valley and Ridge, the Blue Ridge, the Piedmont, and the Coastal Plain are the regions that extend from northwest to southeast in the state. This last region, the Coastal Plain, is located seaward of the Fall Line and is subdivided into three physiographic sections called Sea Island and East Gulf Coastal Plain Section, East Gulf Coastal Plain section, and Sea Island section, located north, southwest, and southeast respectively, of the Coastal Plain region.

In addition, Major Land Resource Areas (MLRA), also known as soil provinces, can be identified for these areas as shown in Table 4-1. The boundaries of the MLRAs correspond closely with the boundaries of the physiographic regions above the Fall Line while they differ below the Fall Line. Below the Fall Line, Table 4-1 indicates the corresponding portions of the MLRAS that fall within the physiographic regions.

Table 4-1. Locations by physiographic and MLRA regions.

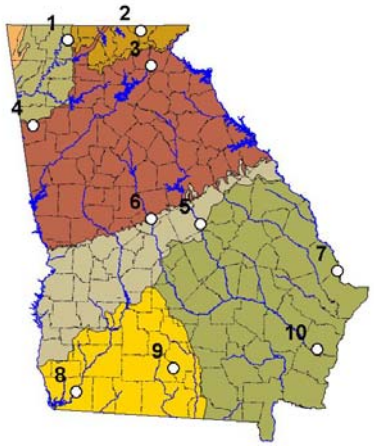

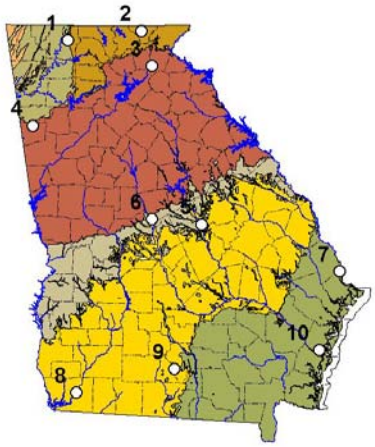

Physiography
- Cumberland Plateau Section
- East Gulf Coastal Plain Section
- Sea Island Section
- Sea Island and East Gulf Coastal Plain Section
- Southern Blue Ridge Section
- Southern Piedmont Section
- Southern Valley and Ridge Section

Major Land Resource Areas
- ATLANTIC COAST FLATWOODS
- BLACK LANDS
- BLUE RIDGE
- SAND HILL
- SAND MOUNTAIN
- SOUTHERN APPALACHIAN
- SOUTHERN COASTAL PLAIN
- SOUTHERN PIEDMONT

Physiographic Region	MLRA
The Valley and Ridge	Southern Appalachian
The Blue Ridge	Blue Ridge
The Piedmont	Southern Piedmont and small north part Sand Hill approximately the Fall Line
Sea Island and East Gulf Coastal Plain Section	Approximately Sand Hill
East Gulf Coastal Plain Section	Western part of Southern Coastal Plain
Sea Island Section	Eastern part of Southern Coastal Plain and Atlantic Coast Flatwoods

Description of the physiographic regions is presented next with geology information, land information and the detailed sediment data obtained from laboratory tests in the context of the geographic setting of the samples.

The Valley and Ridge region, which consists of sedimentary rocks, is located in the northwest section of the state and covers approximately 730,000 hectares (1.80 million acres). The sediments found in this region are underlain by limestone, sandstone, and shale. Elevation varies from 460 meters above sea level (1,500 ft) to 180 meters above sea level (600 ft). The sample from this region is located on US 411 over Mill Creek in Murray County. The sample taken from the foundation of the bridge from 1 ft to 4 ft deep has three different classifications. From 1 to 2 ft deep, silty clayey sand appears. Then, approximately from 2 to 3 ft deep, the material changes to poorly graded sand with silt. Below these last two layers from 3 to 4 ft deep, silty sand material is found. See Table 4-2.

Table 4-2 also shows the critical shear stress values found from the experiments. In this sample from Murray County, the top layer of material is classified as silty, clayey sand, which has a considerably high content of fine material (silt 31%, clay 15%). Its critical shear stress could not be determined because it has a critical shear stress value greater than 21 Pa (the maximum shear stress that can be measured in the experimental apparatus). The next material is a transition material that went from having almost no erosion to having erosion under low shear stresses (less than 3 Pa). This poorly graded sand with silt material is located between two layers with totally different classifications. The last material buried from 3 ft to 4 ft is silty sand with a critical shear stress value of 4 Pa.

Table 4-2. Results of erosion tests and soil property tests on Murray County sample.

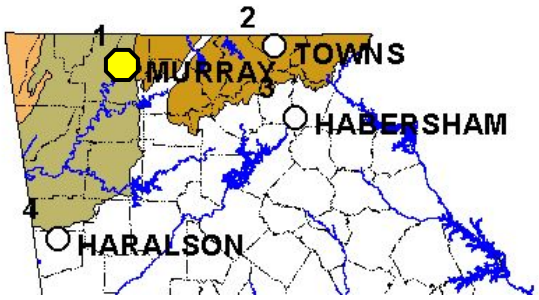

Site	Murray 1'-2'	Murray 2'-3'	Murray 3'-4'
Critical Shear Stress (Pa)	>21	<3	4.05
Sediment	SC-SM	SP-SM	SM
Group Name	Silty, Clayey Sand	Poorly Graded Sand with Silt	Silty Sand
Color	Light Brown	Gray	Light Gray
Dry Density (Kg/m^3)	*1693*	*1695*	*1649*
e (void ratio)	*0.56*	*0.55*	*0.59*
Bulk Density (Kg/m^3)	*1993*	*1963*	*2220*
Water Content	*18%*	*16%*	*35%*
Specific Gravity	*2.64*	*2.62*	*2.63*
Organic Matter	*3.1%*	*1.6%*	*2.4%*
Liquid Limit	*22%*	*NP*	*NP*
Plasticity Index	*5%*	*NP*	*NP*
d_{50} (mm)	*0.0802*	*0.6734*	*0.3112*
Sand	*55%*	*90%*	*75%*
Silt	*31%*	*7%*	*18%*
Clay	*15%*	*3%*	*7%*

The Blue Ridge region consists of metamorphic rocks, and it is located in the northeastern section of the state. The area of this region is approximately 480,000 hectares (1.19 million acres) and its elevation ranges from 1,460 meters above sea level (4,800 ft) to 215 meters above sea level (700 ft). The sample from Towns County is located in this region at SR 288 over Fodder Creek. From this site, 4 sediments were classified between 5 ft and 8 ft deep beneath the surface. The first layer, from 5 ft to 5 ft-6 in., was sandy silt. Next, from 5 ft -6 in. to 6 ft, elastic silt with sand was found. From 6 to 7 ft, sandy silt appeared. The last layer, from 7 to 8 ft, was poorly graded sand with gravel. See Table 4-3.

What appears to be a trend in materials in both the Valley and Ridge and Blue Ridge regions is repeated in this site. Material with higher erosional strength is located on top of a low strength coarse material. First, sandy silt with critical shear stress of 17 Pa is found, followed by elastic silt with sand, with an erosional strength above 21 Pa. The third layer is again sandy silt, the same as the first layer but with less erosional strength (11 Pa). Last, poorly graded sand with gravel having a critical shear stress of about 7 Pa is found.

Table 4-3. Results of erosion tests and soil property tests on Towns County sample.

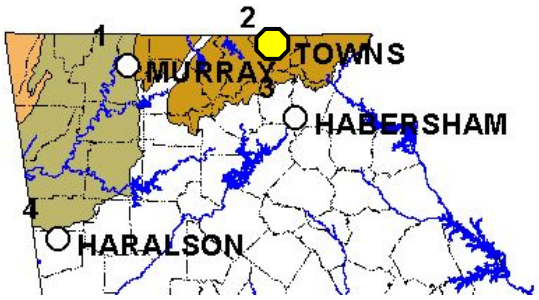

Site	Towns 5' - 5' 6"	Towns 5' 6" - 6'	Towns 6' – 7'	Towns 7' - 8'
Critical Shear Stress (Pa)	17.21	>21	11.31	6.82
Sediment	ML	MH	ML	SP
Group Name	Sandy Silt	Elastic Silt with Sand	Sandy Silt	Poorly Graded Sand with Gravel
Color	Gray Brown	Gray Brown	Gray Brown	Light Brown
Dry Density (Kg/m^3)	*1099*	*876*	*1019*	*1588*
e (void ratio)	*1.44*	*2.03*	*1.68*	*0.71*
Bulk Density (Kg/m^3)	*1477*	*1177*	*1369*	*2079*
Water Content	*34%*	*-*	*34%*	*31%*
Specific Gravity	*2.68*	*2.65*	*2.73*	*2.71*
Organic Matter	*3.6%*	*2%*	*2%*	*1%*
Liquid Limit	*44%*	*51%*	*41%*	*NP*
Plasticity Index	*12%*	*13%*	*7%*	*NP*
d_{50} (mm)	*0.032*	*0.020*	*0.047*	*1.19*
Sand	*44%*	*37%*	*50%*	*97%*
Silt	*36%*	*39%*	*33%*	*3%*
Clay	*20%*	*24%*	*17%*	*0%*

The sediments from the Piedmont region are located over metamorphic rocks and are mostly clayey with kaolinitic mineralogy. The Piedmont extends from the Valley and Ridge and Blue Ridge region to the Fall Line, covering approximately 4.73 million hectares (11.7 million acres) with elevation ranging from 460 m above sea level (1,500 ft) to 153 m above sea level (500 ft). Three of the bridge sites chosen for sampling are located in this region. The first site is Duncan Bridge Rd. over the Chattahoochee River in Habersham County, where five types of sediments were differentiated. From 10 to 11 ft deep and 11 to 12 ft deep, sandy silt is present. From 12 ft to 12 ft-6 in. and from 12 ft-6 in. to 14 ft deep, silty sand materials are found. The last sediment layer is at a depth of 20 ft to 21 ft-6 in. deep and consists of poorly graded sand with silt.

Table 4-4 shows the sediment properties and the values of the measured critical shear stresses. The critical shear stresses show a trend similar to the samples from Towns and Murray Counties, with very erosion resistant sediment on top and weak material below. In this sample obtained from Habersham County, a continuous layer from 10 ft to 14 ft was tested along with an additional Shelby tube taken from 20 ft to 21 ft-6 in.. The first layer, classified as sandy silt, has an erosional strength greater than 21 Pa. The second layer, also classified as sandy silt, has a critical shear stress of 17 Pa. Below these two layers, two silty sand layers with erosional strengths of 3 and 4.5 Pa were found. The sample from 20 ft to 21 ft-6 in. was found to be poorly graded sand with silt having a critical shear stress of around 2.5 Pa. This last value was found by visual observation but the erosion rate relationship could not be measured because of the heterogeneity of the sample.

Table 4-4. Results of erosion and soil property tests on Habersham County sample.

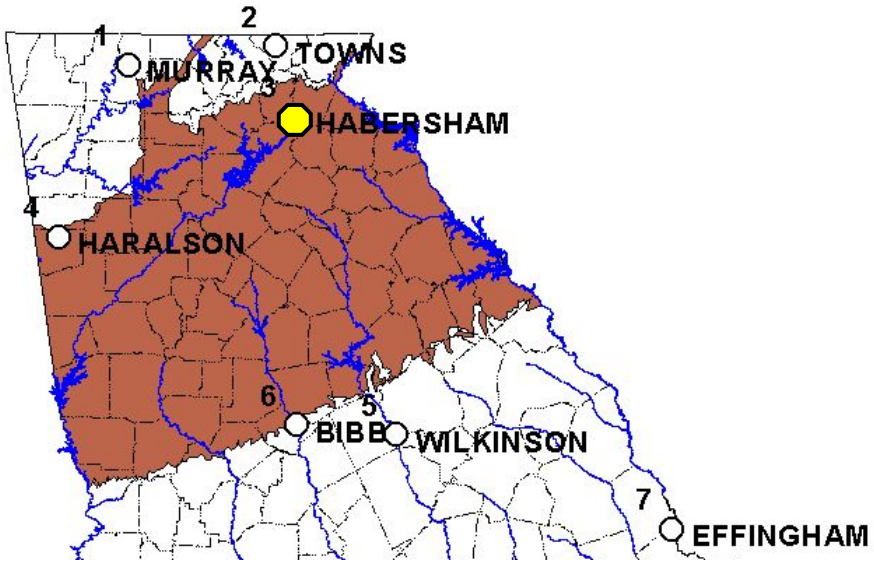

Site	Habersham 10' - 11'	Habersham 11' - 12'	Habersham 12' – 12' 6"	Habersham 12' 6" - 14'	Habersham 20' - 21' 6"
Critical Shear Stress (Pa)	>21	17.35	3.29	4.54	~2.5
Sediment	ML	ML	SM	SM	SP-SM
Group Name	Sandy Silt	Sandy Silt	Silty Sand	Silty Sand	Poorly Graded Sand with Silt
Color	Light Brown	Light Brown	Tan	Tan	Gray
Dry Density (Kg/m^3)	*1410*	*1473*	*1366*	*1463*	*1586*
e (void ratio)	*0.89*	*0.91*	*0.98*	*0.81*	*0.71*
Bulk Density (Kg/m^3)	*1819*	*1909*	*1678*	*1893*	*1962*
Water Content	*29%*	*30%*	*23%*	*29%*	*24%*
Specific Gravity	*2.66*	*2.81*	*2.71*	*2.65*	*2.71*
Organic Matter	*5.5%*	*4%*	*2%*	*2%*	*3%*
Liquid Limit	*35%*	*37%*	*NP*	*NP*	*NP*
Plasticity Index	*11%*	*11%*	*NP*	*NP*	*NP*
d_{50} (mm)	*0.031*	*0.043*	*0.153*	*0.163*	*0.265*
Sand	*46%*	*48%*	*78%*	*83%*	*92%*
Silt	*32%*	*32%*	*14%*	*11%*	*7%*
Clay	*22%*	*20%*	*8%*	*5%*	*1%*

The second site in the Piedmont region is located on US 27 over the Tallapoosa River in Haralson County. Three types of sediments can be described ranging from 12 to 17 ft deep at the foundation of the bridge. From 12 ft to 15 ft-5 in. and from 15 ft-5 in. to 15 feet-7 in., silty sand material is discovered. Underneath these two layers, from 15 ft-7 in. to 17 ft the material changes to sandy silt. See Table 4-5 for detailed sediment information.

This sample from Haralson County was the first sample to be tested in the flume. For that reason, the material located in the middle layer was tested under a maximum shear stress condition of 12 Pa and could not be eroded. After recognizing the need for greater applied shear stresses, additional flow conditions were calculated and a new maximum of 21 Pa was set for the experiments as described previously in Chapter III. The values of the critical shear stresses for the top layer and bottom layer are 6 Pa and approximately 3 Pa, respectively.

Table 4-5. Results of erosion tests and soil property tests on Haralson County sample.

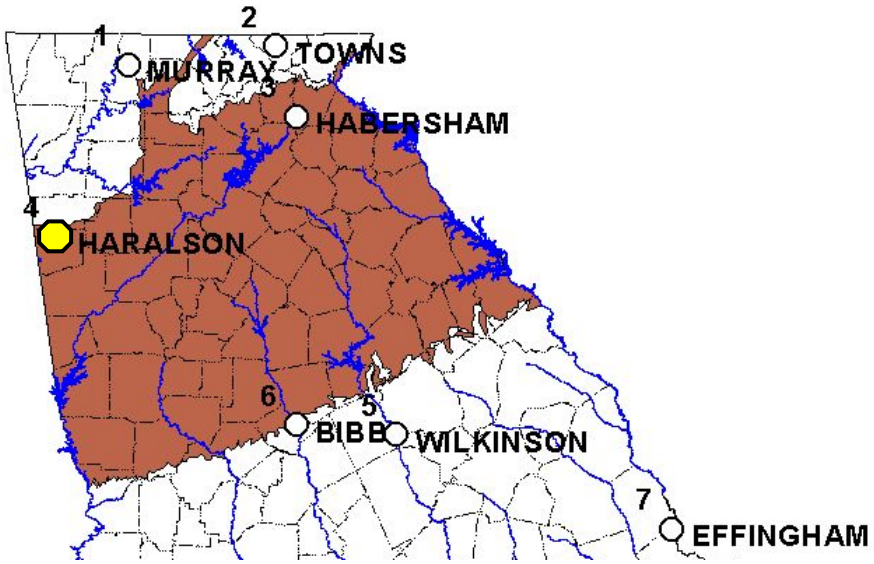

Site	Haralson 12'-15'5"	Haralson 15'5"-15'7"	Haralson 15'7"-17'
Critical Shear Stress (Pa)	5.77	>12	~3
Sediment	SM	SM	ML
Group Name	Silty Sand	Silty Sand	Sandy Silt
Color	Mustard Yellow	Yellow Orange	Tan
Dry Density (Kg/m^3)	*1638*	*1843*	-
e (void ratio)	*0.63*	*0.45*	-
Bulk Density (Kg/m^3)	*2026*	*2279*	-
Water Content	*24%*	-	-
Specific Gravity	*2.67*	*2.68*	*2.82*
Organic Matter	*2.0%*	*1.3%*	*3.0%*
Liquid Limit	*35%*	*29%*	*32%*
Plasticity Index	*9%*	*5%*	*4%*
d_{50} (mm)	*0.27*	*0.44*	*0.04*
Sand	*71%*	*69%*	*48%*
Silt	*27%*	*28%*	*51%*
Clay	*3%*	*3%*	*1%*

The third site in the Piedmont is located near the Fall Line on US 80 / 5th St. over the Ocmulgee River in Bibb County. The MLRA region is called Sand Hill, which consists of deep sandy sediments. Five types of sediments are found at this site, from 25 ft to 32 ft deep. Lean clay with sand is found first from 25 ft to 25 ft-8 in.. Silty sand is then found from 25 ft-8 in. to 27 ft. There is a gap in the material collected between 27 ft and 30 ft. From 30 ft to 30 ft-8 in. the material is classified as clayey sand. Below this layer, poorly graded sand with silt is found from 30 ft-8 in. to 31 ft-4 in.. Finally, a sandy silt layer occurs from 31 ft-4 in. to 32 ft. See Table 4-6 for detailed sediment information.

This highly heterogeneous material collected from Bibb County showed varied critical shear stress values as well. The critical shear stress value found for the first layer was almost 10 Pa. This value decreased to approximately 2.5 Pa for the next layer. After the jump to 30 ft deep, the material found was stronger than the layer above it and its value of critical shear stress increased to approximately 16.5 Pa. Underneath this last layer, the material dropped in erosional strength again to 3 Pa. Finally, the last layer had a critical shear stress value of 5 Pa, slightly stronger than the overlying layer.

Table 4-6. Results of erosion tests and soil property tests on Bibb County sample.

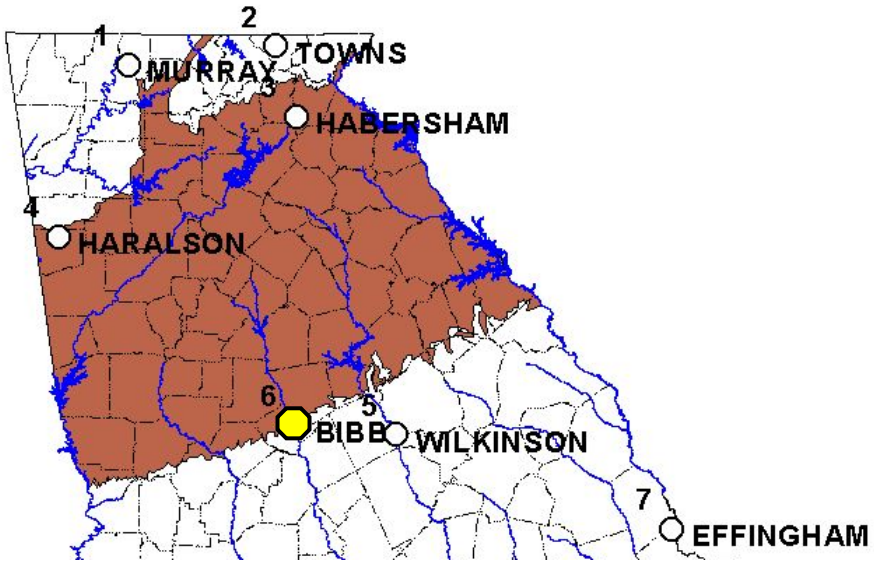

Site	Bibb 25' - 25' 8"	Bibb 25' 8" – 27'	Bibb 30' - 30' 8"	Bibb 30' 8" - 31' 4"	Bibb 31' 4" - 32'
Critical Shear Stress (Pa)	9.68	~2.5	~16.5	3.32	5.11
Sediment	CL	SM	SC	SP-SM	ML
Group Name	Lean Clay with Sand	Silty Sand	Clayey Sand	Poorly Graded Sand with Silt	Sandy Silt
Color	Light Brown	Gray	Light Brown	Light Brown	Dark Gray
Dry Density (Kg/m^3)	*1261*	*1631*	*1596*	*1316*	*1162*
e (void ratio)	*1.07*	*0.62*	*0.68*	*1.02*	*1.19*
Bulk Density (Kg/m^3)	*1749*	*1949*	*1973*	*1715*	*1513*
Water Content	*39%*	*20%*	*24%*	*30%*	
Specific Gravity	*2.62*	*2.64*	*2.69*	*2.66*	*2.54*
Organic Matter	*10.3%*	*6.5%*	*6.7%*	*6.2%*	*16.4%*
Liquid Limit	*36%*	*NP*	*32%*	*NP*	*39%*
Plasticity Index	*18%*	*NP*	*11%*	*NP*	*12%*
d_{50} (mm)	*0.0074*	*0.250*	*0.111*	*0.159*	*0.036*
Sand	*26%*	*84%*	*59%*	*90%*	*44%*
Silt	*40%*	*9%*	*20%*	*4%*	*33%*
Clay	*34%*	*7%*	*21%*	*6%*	*23%*

The last geologic region considered is the Coastal Plain. This large region covers approximately 9.38 million hectares (23.2 million acres) and can be subdivided in three physiographic districts: Sea Island and East Gulf Coastal Plain section (2.1 million hectares), Sea Island section (5.1 million hectares), and East Gulf Coastal Plain section (2.2 million hectares). In addition to this subdivision, according to the major land resource areas, it can be subdivided into Sand Hill, Southern Coastal Plain, and Atlantic Coast Flatwoods regions. Five bridge sites are located in this region.

The first site in the Coastal Plain region is located at SR 57 over the Oconee River in Wilkinson County. It is located in the Sea Island and East Gulf Coastal Plain physiographic Section and in the Southern Coastal Plain MLRA. The material from this site is classified as poorly graded sand with silt from 36 ft-6 in. to 37 ft-6 in., and below that silty clay from 37 ft-6 in. to 38 ft-6 in.. Table 4-7 summarizes the sediment test results.

The critical shear stress values found for the two types of material found in this site can also be seen in Table 4-7. The poorly graded sand with silt top layer has a critical shear stress value of 0.44 Pa. The lower layer, which was classified as fat clay could not be eroded. The critical shear stress for this last layer is greater than 21 Pa.

Table 4-7. Results of erosion tests and soil property tests on Wilkinson County sample.

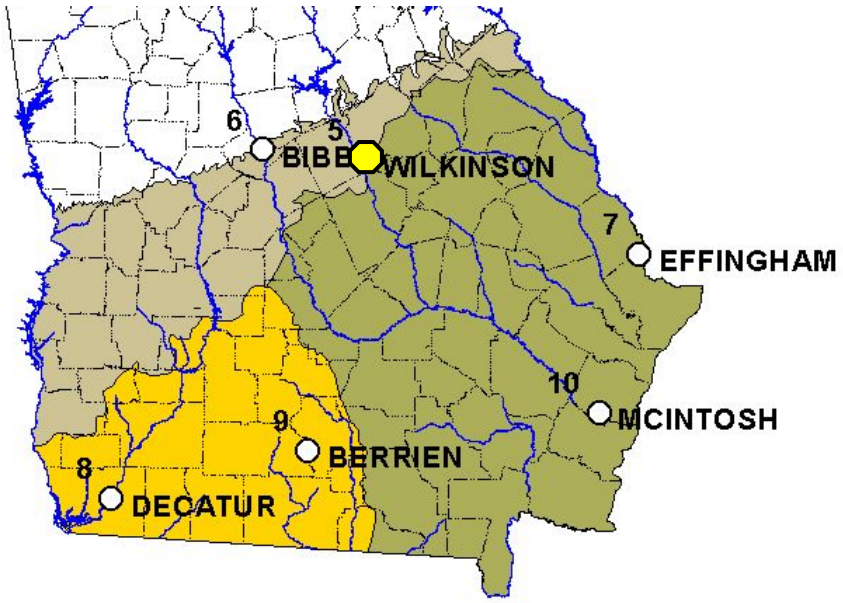

Site	Wilkinson 36'6"-37'6"	Wilkinson 37'6"-38'6"
Critical Shear Stress (Pa)	0.44	>21
Sediment	SP-SM	CH
Group Name	Poorly Graded Sand with Silt	Fat Clay
Color	Tan	Light Brown
Dry Density (Kg/m^3)	1544	1657
e (void ratio)	0.70	0.58
Bulk Density (Kg/m^3)	2007	2227
Water Content	30%	34%
Specific Gravity	2.63	2.61
Organic Matter	0.3%	6.6%
Liquid Limit	NP	51%
Plasticity Index	NP	23%
d_{50} (mm)	0.1803	0.004
Sand	93%	11%
Silt	3%	49%
Clay	4%	40%

The second sample collected from the Coastal Plain is located in Effingham County at the I-95 bridge over the Savannah River. This site lies in the Sea Island physiographic region and in the Atlantic Coast Flatwoods. The material is classified as clayey sand from 20 ft to 21 ft, and poorly graded sand from 21 ft to 22 ft. See details in Table 4-8.

The critical shear stress value for the material on top is greater than 21 Pa. The material underneath the top clayey sand is classified as poorly graded sand and has a critical shear stress of 3 Pa.

Table 4-8. Results of erosion tests and soil property tests on Effingham County sample.

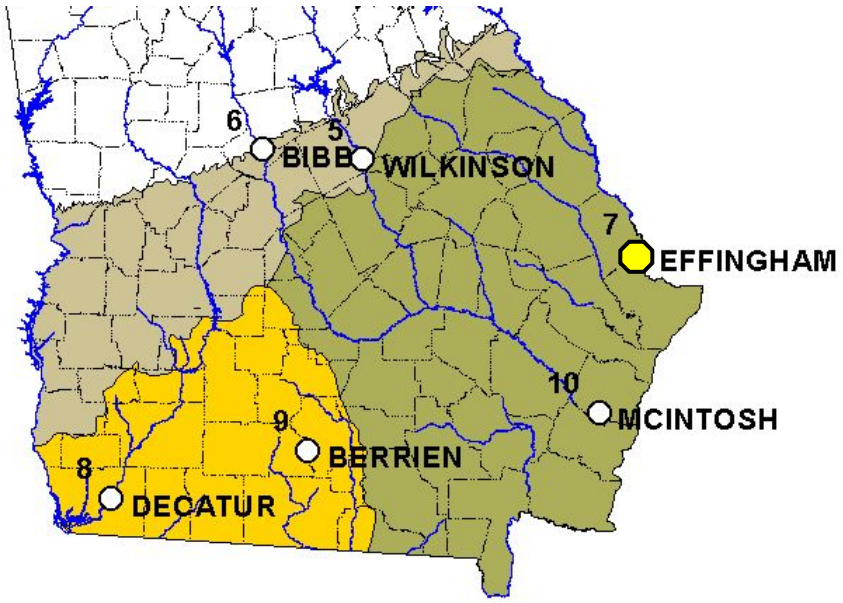

Site	Effingham 20'-21'	Effingham 21'-22'
Critical Shear Stress (Pa)	>21	3.24
Sediment	SC	SP
Group Name	Clayey Sand	Poorly Graded Sand
Color	Gray	Light Gray
Dry Density (Kg/m^3)	*1430*	-
e (void ratio)	*0.78*	-
Bulk Density (Kg/m^3)	*1733*	-
Water Content	*21%*	*21%*
Specific Gravity	*2.54*	*2.64*
Organic Matter	*2.2%*	*0.0%*
Liquid Limit	*36%*	*NP*
Plasticity Index	*19%*	*NP*
d_{50} (mm)	*0.3*	*0.45*
Sand	*67%*	*99%*
Silt	*15%*	*1%*
Clay	*18%*	*0%*

The sample collected from Decatur County, SR 1b / Calhoun St. over the Flint River, is located in the East Gulf Coastal Plain physiographic region and in the Southern Coastal Plain MRLA. It is classified as clayey sand from 20 ft to 20 ft-4 in.. Below this layer, a silty sand is found from 20 ft 4 in. to 22 ft. See Table 4-9 for details.

The measured critical shear stress value for the top layer is 8 Pa. The second layer is heterogeneous and its approximate critical shear stress value is 2.5 Pa.

Table 4-9. Results of erosion tests and soil property tests on Decatur County sample.

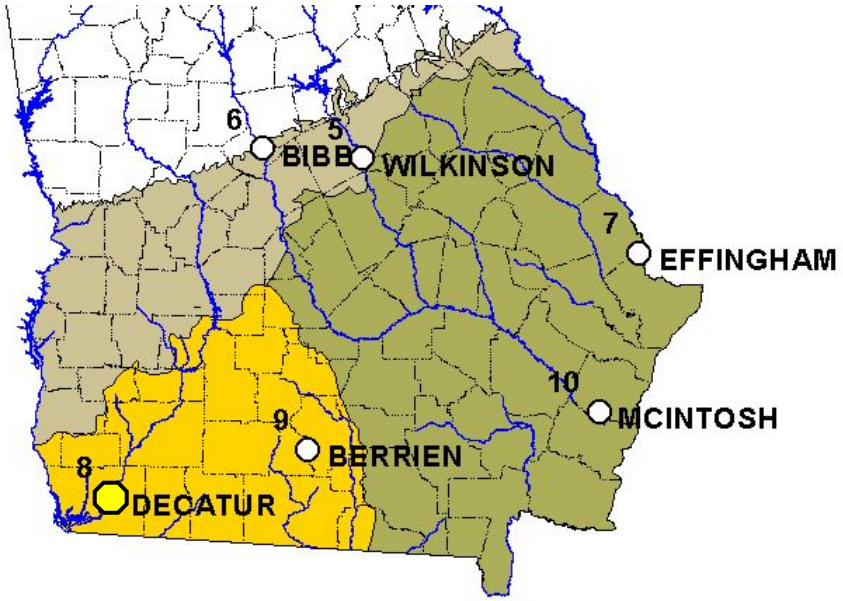

Site	Decatur 20'-20'4"	Decatur 20'4"-22'
Critical Shear Stress (Pa)	7.90	~2.5
Sediment	SC	SM
Group Name	Clayey Sand	Silty Sand
Color	Red Brown	Brown
Dry Density (Kg/m^3)	*1761*	*1548*
e (void ratio)	*0.49*	*0.71*
Bulk Density (Kg/m^3)	*2114*	*1887*
Water Content	*20%*	*22%*
Specific Gravity	*2.62*	*2.65*
Organic Matter	*4.8%*	*0.6%*
Liquid Limit	*28%*	*NP*
Plasticity Index	*12%*	*NP*
d_{50} (mm)	*0.131*	*0.404*
Sand	*60%*	*83%*
Silt	*9%*	*3%*
Clay	*31%*	*14%*

The fourth site in this Coastal region was collected in Berrien County in the East Gulf Coastal Plain physiographic section and in the Southern Coastal Plain MLRA. Four layers were identified for this site. First, sandy fat clay sediment from 25 ft to 25 ft-6 in. is found. Clayey sand forms the second layer from 25 ft-6 in. to 27 ft. This layer is followed by a jump in sampling depth to a silty sand from 30 ft to 30 ft-6 in. Last, fat clay with sand is underneath from 30 ft 6 in. to 32 ft. See Table 4-10 for the complete sediment properties.

All these four sediment layers were found to have high fine material content. For two of these sediments, the extreme top and the extreme bottom, the median size could not be determined from hydrometer analysis given that more than 50 percent of the material was still suspended after the end of the test. None of these four materials could be eroded under the maximum shear stress flow condition. The sediment samples collected from Berrien County have the highest erosional strength of all the samples tested in this study.

Table 4-10. Results of erosion tests and soil property tests on Berrien County sample.

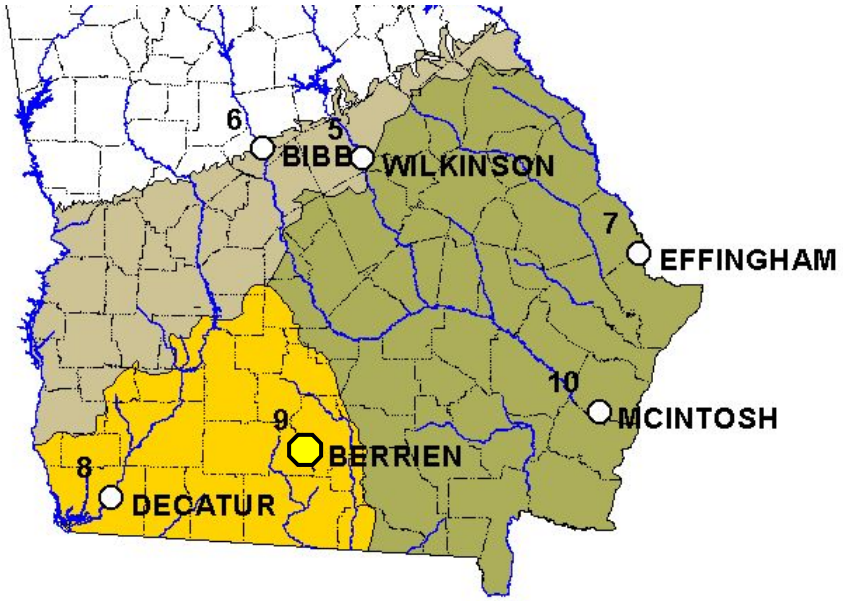

Site	Berrien 25'-25'6"	Berrien 25'6"-27'	Berrien 30'-30'6"	Berrien 30'6"-32'
Critical Shear Stress (Pa)	>21	>21	>21	>21
Sediment	CH	SC	SM	CH
Group Name	Sandy Fat Clay	Clayey Sand	Silty Sand	Fat Clay with Sand
Color	Gray Tan	Light Gray	Brown	Gray
Dry Density (Kg/m^3)	*1065*	*1246*	*1482*	*1052*
e (void ratio)	*1.55*	*1.05*	*0.74*	*1.56*
Bulk Density (Kg/m^3)	*1698*	*1895*	*1764*	*1716*
Water Content	*59%*	*52%*	*19%*	*63%*
Specific Gravity	*2.72*	*2.55*	*2.58*	*2.7*
Organic Matter	*4.6%*	*6.1%*	*5.6%*	*4.3%*
Liquid Limit	*103%*	*76%*	*22%*	*114%*
Plasticity Index	*72%*	*39%*	*2%*	*69%*
d_{50} (mm)	*<0.001*	*0.084*	*0.144*	*<0.001*
Sand	*38%*	*53%*	*72%*	*26%*
Silt	*5%*	*23%*	*10%*	*6%*
Clay	*57%*	*24%*	*18%*	*68%*

The last site is located on US 17 over the Darien River in McIntosh County in the Sea Island physiographic region and in the Atlantic Coast Flatwoods. This material was found to be clayey sand with gravel (shells). This black material had large particles, possibly of calcareous origin, such as shells. See details of the sediment properties in Table 4-11.

The critical shear stress of this material collected from McIntosh County was found to be 17.2 Pa. This material had negligible surface erosion and its critical shear stress value was found when mass erosion was observed. This abrupt change from no erosion to large erosion rates happened in part due to the existence of shell-like particles that led to chunks as big as the shells to be easily dislodged.

Table 4-11. Results of erosion tests and soil property tests on McIntosh County sample.

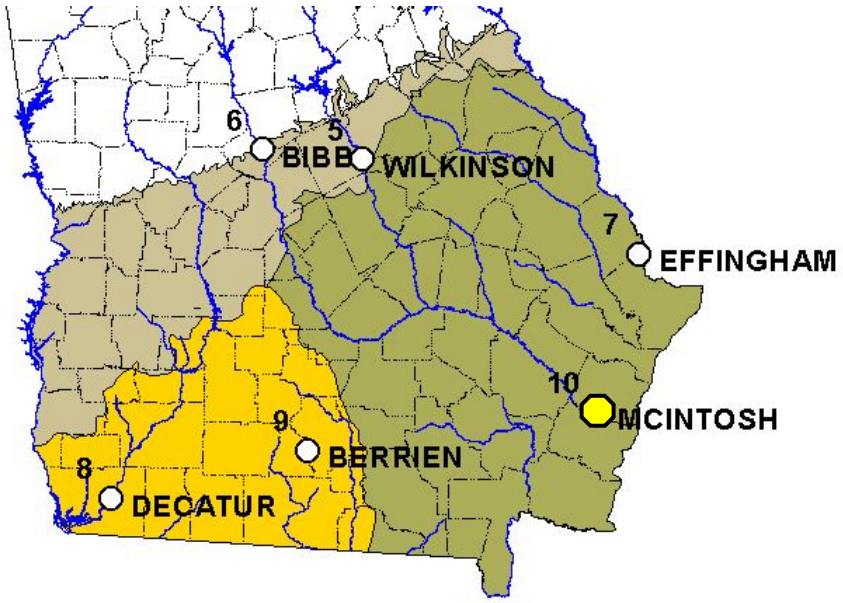

Site	McIntosh 10'-12'
Critical Shear Stress (Pa)	17.17
Sediment	SC
Group Name	Clayey Sand with Gravel (Shells)
Color	Black
Dry Density (Kg/m^3)	*1298*
e (void ratio)	*1.00*
Bulk Density (Kg/m^3)	*1728*
Water Content	*33%*
Specific Gravity	*2.6*
Organic Matter	*5.7%*
Liquid Limit	*32%*
Plasticity Index	*16%*
d_{50} (mm)	*1*
Sand	*87%*
Silt	*6%*
Clay	*7%*

4.2 Erosion Relationships

Numerous researchers have found experimental relationships for erosion rates as a function of flow conditions and sediment properties, some of which have been referenced in Chapter II. The approach taken in this study is to separate the role of the flow conditions from the role of the soil properties, dealing with each one in two steps. In the first step, the erosion-rate response of the sediments is measured under applied shear stresses that produce erosive flow conditions. Then, the results obtained are correlated with the soil properties in order to identify any dependence.

A selection of relationships is presented in Chapter II, particularly the set of equations in Table 2-2, which are the results of previous experimental studies for fine-grained material erodibility. The most common models are excess shear stress relationships. Excess shear stress relationships include the influence of the flow conditions, represented by the applied shear stress, and the influence of soil properties represented by the critical shear stress. Other constants included in the model can be influenced by both flow conditions and soil properties.

Three relationships were explored: linear, exponential and power. Two of them, linear and exponential, showed the best agreement with the experimental data and were included in the analysis based on their goodness of fit and the standard error of the erosion parameters. For those relationships, seventeen sediment samples out of the thirty-one samples on which soil classification tests were performed had acceptable erosion rate vs. applied shear stress relationships. An acceptable relationship was defined

as one having a coefficient of determination greater than 0.50 ($R^2 > 0.50$). This criterion was applied to the two best regression models, which were piecewise linear and exponential relationships.

The linear regression model or piecewise linear regression model, showed good agreement with the data. This type of model is certainly easier to manipulate and fewer parameters have to be defined, which makes it more robust to apply in predictions. However, the range of applicability of the linear models is more limited. For larger ranges of shear stress values, piecewise models are required, although this increases the number of parameters to measure. The location of the break point for the piecewise linear model is based on judgment applied to the plotted data and on maximizing the coefficients of determination of each segment. Linear models are preferred for low increments of the applied shear stresses beyond the critical value and they are more accurate in finding the critical shear stress values using the first part of the model for the piecewise relationships.

The exponential model describes a more realistic shape of the erosion rate function over the full range of low to high shear stresses. This model is asymptotic to the shear stress axis and an additional variable, the critical erosion rate, has to be defined. The critical erosion rate value acts as an axis intercept for the model in order to find the critical shear stress. The value of the critical erosion rate can be set to satisfy the physical restriction of the minimum laboratory erosion rate that can be measured in the laboratory apparatus, as

well as to provide a consistent intercept for determining the critical shear stress in the exponential model.

In order to provide consistency between the piecewise linear and exponential models, the critical erosion rate was varied to minimize the difference between the critical shear stress values for the two models. The resulting value of the critical erosion rate was found to be 0.0019 kg/m^2/s, which is greater than the minimum erosion rate measured using this setup, 0.001 kg/m^2/s. The minimum erosion rate is based on running the flume test for three hours, and it can be decreased as long as the running time is extended. However, given that the minimum value is less than the computed critical erosion rate, more precision is not necessary.

In summary, the best two models were found to be the piecewise linear and exponential models as given by Equations 3.13 and 3.14. The piecewise linear model gives the best performance in calculating the critical shear stress and estimating low erosion rates. The exponential model is best to apply for the full shear stress range. Thus, the procedure presented utilizes the best attributes of both models such that a full range of the soil response can be described when given the soil properties and the flow conditions.

Figure 4-1 shows the erosion test results for the first group of sediments for which measured erosion rates reached 1.1 kg/m^2/s. The solid lines are the linear and piecewise linear models, and the dashed lines are the exponential models. Each sample is identified

by the county in which it is located as given previously in Table 3-1 and by the depth of the sample layer.

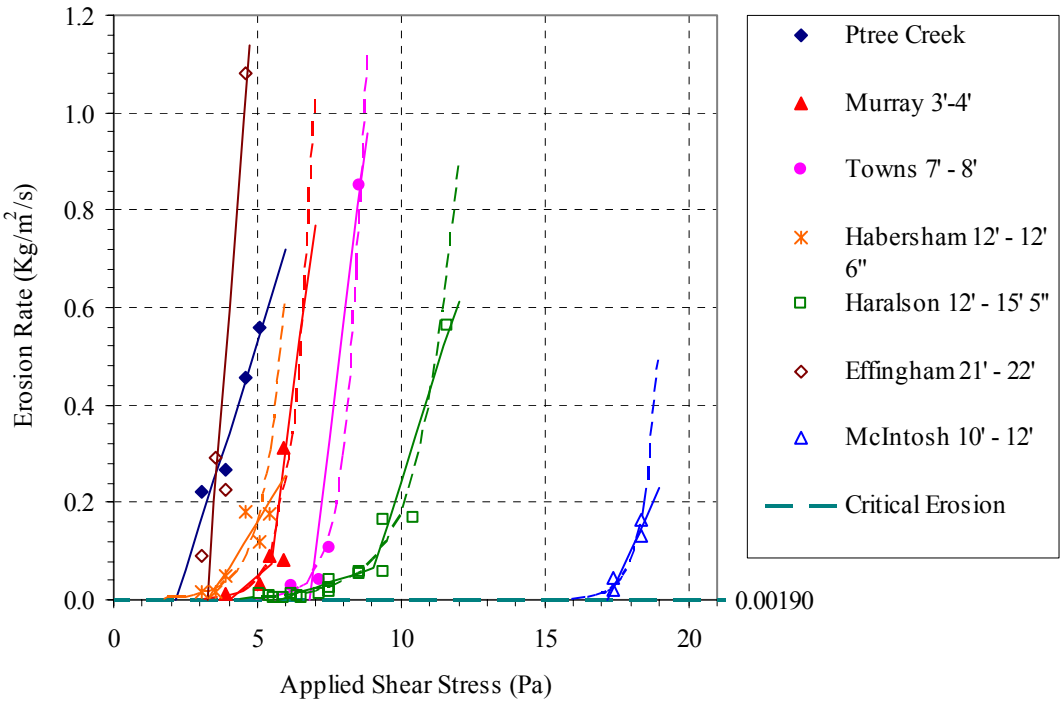

Figure 4-1. Erosion rate vs. applied shear stress relationships for materials with erosion rates up to 1.1 kg/m^2/s.

Figure 4-2 shows the measured erosion rates and their best-fit models for erosion rates up to 0.06 kg/m^2/s. In some cases, the data follow a single linear relationship rather than a piecewise linear one.

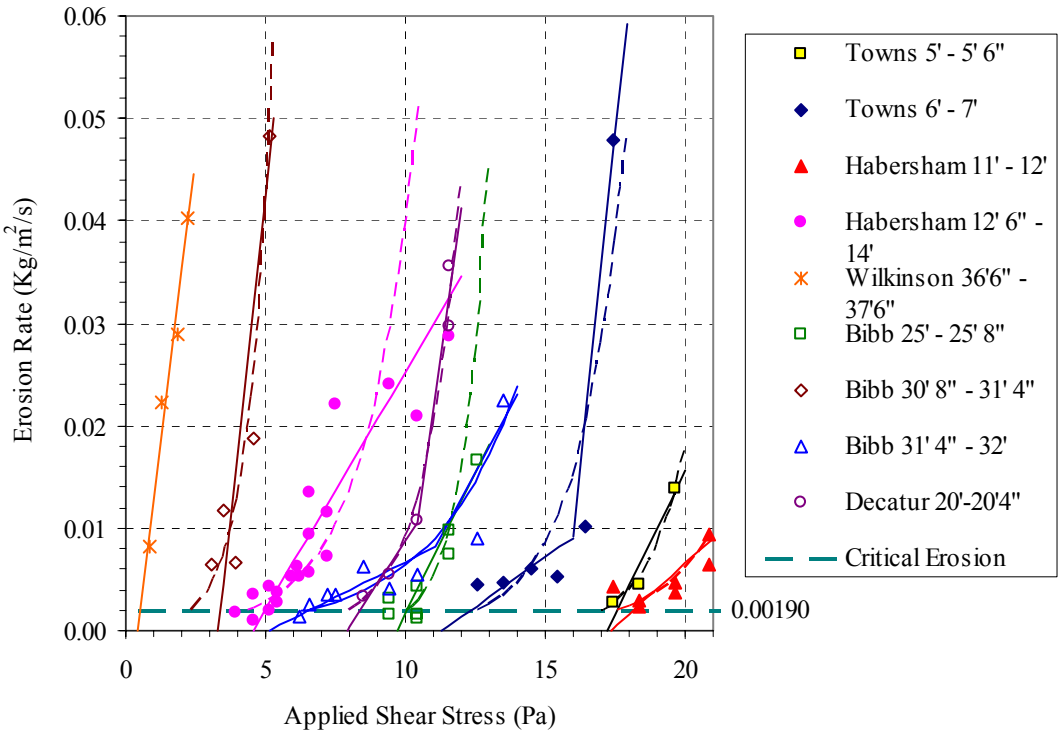

Figure 4-2. Erosion rate vs. applied shear stress relationships for materials with erosion rates up to 0.06 kg/m^2/s.

The regression coefficients in terms of critical shear stress and erosion rate constant are given in Tables 4-12 and 4-13, respectively, for both the linear and exponential regression models illustrated in Figures 4-1 and 4-2. The standard error in the critical shear stress has an average value of 0.45 Pa for the linear model and 0.57 Pa for the exponential model, as shown in Table 4-12. In some cases, the exponential model could not be used because the data fit a single straight line very closely. The average coefficient of determination, R^2, was 0.80 for the linear model and 0.84 for the exponential model as given in Table 4-12.

Table 4-12. Linear, piecewise linear and exponential critical shear stress values for the erosion rate vs. applied shear stress models.

	Linear			Exponential		
	$E = M \cdot \left(\frac{\tau - \tau_c}{\tau_c} \right)$			$E = E_c \cdot e^{a \cdot \left(\frac{\tau - \tau_c}{\tau_c} \right)}$		
Critical Erosion = 0.00190 kg/m^2/s	**τ_c, Pa**	**s.e. τ_c**	**R^2**	**τ_c, Pa**	**s.e. τ_c**	**R^2**
Sand d_{50}=1.16mm (1)	1.03	0.15	0.95	0.38	0.20	0.95
Sand d_{50}=1.16mm (2)	2.91	0.04	0.99			
Peachtree Creek	2.18	0.43	0.92			
Murray 3'-4' (1)	4.05	0.50	0.75	3.14	0.63	0.81
Murray 3'-4' (2)	5.33	0.29	0.44			
Towns 5'-5'6"	17.21	0.48	0.91	17.02	0.26	0.98
Towns 6'-7' (1)	11.31	1.44	0.65	12.55	0.95	0.68
Towns 6'-7' (2)	15.62	0.48	0.84			
Towns 7'-8'	6.82	0.39	0.72	4.96	0.62	0.89
Habersham 11'-12'	17.35	0.84	0.57	17.57	0.78	0.56
Habersham 12'-12'6"	3.29	0.32	0.79	1.75	0.55	0.85
Habersham 12'6"-14"	4.54	0.28	0.85	4.35	0.38	0.77
Haralson 12'-15'5" (1)	5.77	0.27	0.70	4.38	0.33	0.89
Haralson 12'-15'5" (2)	8.68	0.33	0.81			
Wilkinson 36'6"-37'6"	0.44	0.14	0.98			
Bibb 25'-25'8"	9.68	0.29	0.79	10.08	0.31	0.66
Bibb 30'8"-31'4"	3.32	0.34	0.73	2.36	0.54	0.79
Bibb 31'4"-32' (1)	5.11	1.00	0.65	6.32	0.56	0.85
Bibb 31'4"-32' (2)	9.45	0.98	0.76			
Effingham 21'-22'	3.24	0.25	0.81			
Decatur 20'-20'4" (1)	7.90	0.36	0.96	7.98	0.17	0.99
Decatur 20'-20'4" (2)	9.88	0.32	0.95			
McIntosh 10'-12'	17.17	0.15	0.94	15.92	0.54	0.88
Average		**0.45**	**0.80**		**0.57**	**0.84**

The values of the erosion rate constants *M* and *a* for the linear and exponential regression models as given by Equations 3-13 and 3-14, respectively, are given in Table 4-13 along with the standard errors of each coefficient. The average relative uncertainty in *M* is 29% while it is 22% for *a*.

Table 4-13. Linear, piecewise linear and exponential slope coefficients for the erosion rate vs. applied shear stress models.

	Linear			**Exponential**		
	$E = M \cdot \left(\frac{\tau - \tau_c}{\tau_c} \right)$			$E = E_c \cdot e^{a \cdot \left(\frac{\tau - \tau_c}{\tau_c} \right)}$		
Critical Erosion = 0.00190 kg/m^2/s	***M*** **kg/m^2/s**	**s.e. *M***	**s.e./*M***	***a***	**s.e. *a***	**s.e./*a***
Sand d_{50}=1.16mm (1)	0.063	0.007	11%	0.626	0.053	8%
Sand d_{50}=1.16mm (2)	1.81	0.11	6%			
Peachtree Creek	0.410	0.083	20%			
Murray 3'-4' (1)	0.209	0.084	40%	5.12	1.45	28%
Murray 3'-4' (2)	2.45	1.95	80%			
Towns 5'-5'6"	0.096	0.030	32%	12.7	1.9	15%
Towns 6'-7' (1)	0.022	0.009	43%	7.6	2.6	34%
Towns 6'-7' (2)	0.41	0.18	44%			
Towns 7'-8'	3.29	1.44	44%	8.2	2.0	25%
Habersham 11'-12'	0.043	0.017	39%	8.3	3.3	40%
Habersham 12'-12'6"	0.309	0.080	26%	2.37	0.49	21%
Habersham 12'6"-14"	0.021	0.002	10%	2.33	0.30	13%
Haralson 12'-15'5" (1)	0.117	0.023	20%	3.5	0.33	9%
Haralson 12'-15'5" (2)	1.60	0.38	24%			
Wilkinson 36'6"-37'6"	0.010	0.001	11%			
Bibb 25'-25'8"	0.053	0.011	21%	11.0	3.2	29%
Bibb 30'8"-31'4"	0.084	0.029	35%	2.74	0.82	30%
Bibb 31'4"-32' (1)	0.007	0.002	33%	2.08	0.33	16%
Bibb 31'4"-32' (2)	0.048	0.019	40%			
Effingham 21'-22'	2.53	0.87	34%			
Decatur 20'-20'4" (1)	0.033	0.007	21%	6.2	0.41	7%
Decatur 20'-20'4" (2)	0.192	0.043	23%			
McIntosh 10'-12'	2.14	0.38	18%	28.7	7.6	26%
Average			29%			22%

4.3 Multiple Linear Regression Analysis

The best group of independent variables for prediction of critical shear stress and the erosion rate constant of the sediment samples was determined using MINITAB statistical software to perform simple and multiple linear regression analysis.

Among the sediment parameters measured for all the sites, the following were included in the statistical analysis: bulk density (kg/m^3), water content (decimal fraction), organic matter content (decimal fraction), median sediment size (mm), clay content (decimal fraction) and fines content, defined as the sum of the clay and silt content (decimal fraction).

The soil parameters that were measured but not included in the statistical analysis were the specific gravity, the liquid limit, and plastic limit. The specific gravity was excluded because of its low variability. The liquid limit and plasticity showed some correlation since, for example, the most resistant material (Berrien Co.) had by far the largest values of liquid and plastic limit. However, only eight of the seventeen data points were classified as plastic material, too few to perform confident regression analysis.

Two basic procedures, best subsets and stepwise regression, were used in order to identify the independent variables that most influence the critical shear stress and regression models that best predict future responses. The best subsets option evaluates all possible subsets of the predictors starting with one-predictor regression models and extending to models that include all variables entered by the user. The stepwise

regression procedure adds or removes predictors depending on their influence on the regression relationship. Parameters without any explanatory value are removed while those parameters that provide the most explanation of the variance are added.

In order to verify the goodness of fit of the models, statistics such as the coefficient of determination, the adjusted coefficient of determination, the Mallow's C_p, and the estimated standard error of the model are evaluated.

The coefficient of determination indicates how close the data points are to the best-fit model. In other words, R^2 (coefficient of determination) is the proportion of the total variability accounted for by the regression line for Y as a function of x. It takes on values from zero, an uncorrelated model, to one (exact model predictability). R^2 is given by

$$R^2 = \frac{SSR}{SST} = 1 - \frac{SSE}{SST} \tag{4.1}$$

in which SSR = sum of squares of explained deviations of predicted values of Y by the regression relationship with respect to the mean value of Y; SSE = sum of squares of unexplained deviations in Y with respected to the regression line; and SST = total sum of squares that measures the total variability in the values of the dependent variable Y. The value of SST is equal to the sum of SSR and SSE, which are given by

$$SST = \sum_{i=1}^{n} \left(y_i - \bar{y} \right)^2 \tag{4.2}$$

$$SSR = \sum_{i=1}^{n} \left(\hat{y}_i - \bar{y} \right)^2 \tag{4.3}$$

$$SSE = \sum_{i=1}^{n} \left(y_i - \hat{y} \right)^2 \tag{4.4}$$

in which y_i = observed value of the dependent variable, $\hat{y}_i$ = fitted value of the dependent variable, $\bar{y}$ = average observed value of the dependent variable, i = observation number, and n = total number of observations.

The adjusted coefficient of determination, R^2 *(adj.)*, differs from R^2 in that the adjusted value accounts for the number of predictors included in the model. When more variables are included in the model, a higher R^2 is obtained (better fit model); however, the predictability value of the model is reduced. R^2 *(adj.)* is a useful statistic that helps to identify the best prediction models. R^2 *(adj.)* is given by

$$R^2\,(adj.) = 1 - \frac{SSE}{SST} \cdot \frac{(n-1)}{(n-k-1)} \tag{4.5}$$

in which n = number of measured data points, and k = number of predictors estimated.

The Mallow's C_p is a measure of how well the model predicts the dependent variable. Models with small C_p and values less than and close to the number of variables included (p) have small variability and good predictability. C_p is given by

$$C_p = \frac{SSE_p}{SSE_{all}/(n - k_{all} - 1)} - (n - 2p) \tag{4.6}$$

in which p = number of predictors included, k_{all} = total number of predictors to include, SSE = sum of squares of error in model with p predictors, SSE_{all} = sum of squares of error with all the predictors, and n = number of measured data points.

The last statistic included in the analysis is the estimated standard deviation of the error, s. This is the average error incurred when using the best-fit regression model. For multiple linear regressions the number of predictors is included so that the error increases as the number of predictors in the model increases. Lower values of this statistic signify a better model. It is given by

$$s = \sqrt{\frac{SSE}{n - k - 1}} \tag{4.7}$$

in which SSE = sum of squares of error between data points and predicted values, n = number of measured data points, and k = number of predictors estimated.

4.4 Critical Shear Stress Dependency on Sediment Properties

The statistics described above are utilized to assess the goodness of fit and the goodness of prediction of a regression model in order to choose the best model. In the first multiple linear regression model considered, the predictors selected are

- bulk density (kg/m^3),
- water content (decimal fraction),
- organic matter (decimal fraction),
- median size (mm),
- clay content (decimal fraction), and
- fines content (decimal fraction).

The response variable is the critical shear stress found using the first segment of the piecewise linear regression model.

For the linear model, one outlier point was identified, which was the sample for McIntosh County. The material from this site can be considered unusual because of its content of shells. After removing this point, the results are given by Table 4-14 in which fines content is the best predictor, followed by organic matter and median sediment size. It should be mentioned that the clay content was expected to be a better predictor variable than fines content given that at clay sizes the change to platelet-like shape magnifies the interparticle forces that also occur for silt sizes. Also, Kamphuis and Hall (1983), who performed initiation of motion tests on consolidated fine sediments, found that the shear stress required to initiate motion increases with increases in the clay content. However, for this data the fines content is a better predictor variable.

Table 4-14. MINITAB output showing the best subsets of predictors for the critical shear stress parameter as the response.

Best Subsets Regression: TcLin versus Bulk, WC, OM, d50, Clay, Fines

Response is TcLin

Vars	R-Sq	R-Sq(adj)	Mallows C-p	S	Bulk	WC	OM	d50	Clay	Fines
1	54.6	51.3	3.1	3.5848						X
1	38.5	34.1	8.4	4.1707					X	
2	70.0	65.4	-0.0	3.0244			X			X
2	56.4	49.7	4.5	3.6449				X		X
3	**71.7**	**64.6**	**1.4**	**3.0570**			**X**	**X**		**X**
3	**70.4**	**63.1**	**1.8**	**3.1237**	**X**		**X**			**X**
4	72.9	63.0	3.0	3.1254	X		X	X		X
4	71.7	61.5	3.4	3.1898		X	X	X		X
5	72.9	59.3	5.0	3.2769	X		X	X	X	X
5	72.9	59.3	5.0	3.2773	X	X	X	X		X
6	72.9	54.9	7.0	3.4529	X	X	X	X	X	X

Given the limited number of data points (16), it was decided to use a maximum of three predictors in a regression model. Considering the values of the model statistics shown in Table 4-14, the models with three variables perform better, and the best model with three predictors is the one with fines, organic matter, and median size. The statistics with these predictors are given in Table 4-14. The best-fit linear model is given by

$$\tau_c = 0.76 + 25.7 \cdot Fines - 61.4 \cdot OM + 2.37 \cdot d_{50} \tag{4.8}$$

in which τ_c = critical shear stress, Pa; *Fines* = decimal fraction of fine material; *OM* = decimal fraction of organic matter; and d_{50} = median size, mm.

The performance of the regression equation is shown in Figure 4-3 in a plot of measured vs. predicted shear stress. The value of R^2 is 0.72 and the standard error of estimate in the critical shear stress is 3.1 Pa which is greater than the estimated experimental uncertainty of 0.5 Pa given previously in Table 4-12. This means that there is additional unexplained variation that cannot be accounted for by the experimental uncertainty.

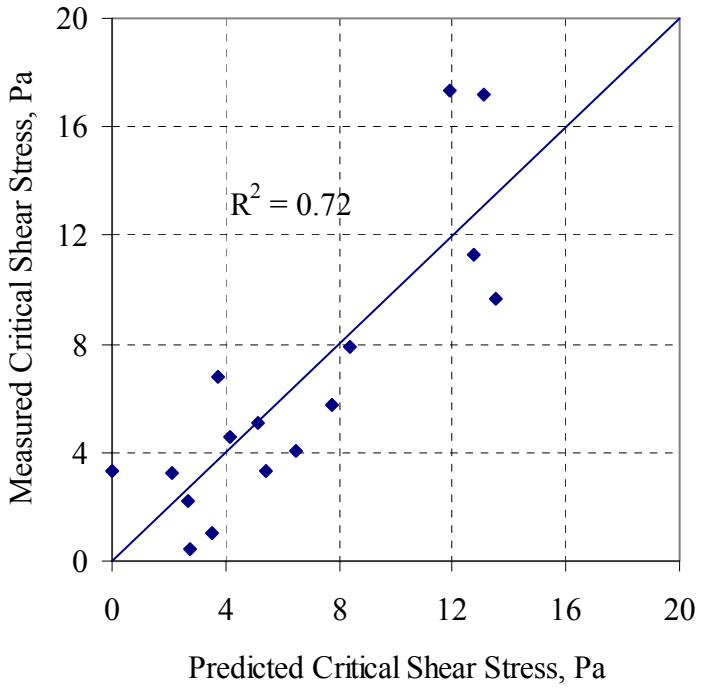

Figure 4-3. Comparison of measured and predicted critical shear stress using a multiple linear model.

Now, considering the other three-parameter model in Table 4-14, bulk density replaces median sediment size as a predictor. The regression equation is given by

$$\tau_c = 5.18 + 22.8 \cdot Fines - 62.8 \cdot OM - 0.00158 \cdot \rho_b \quad (4.9)$$

in which τ_c = critical shear stress in Pa; *Fines* = decimal fraction of fine material; *OM* = decimal fraction of organic matter; and ρ_b = bulk density in kg/m^3.

The value of R^2 = 0.70 which is only slightly less than for Equation 4.8. However, the regression Equation 4.9 shows a decrease in critical shear stress with an increase in the bulk density, which contradicts the results obtained by other researchers (Mehta 1991, Krone 1999, Ravisangar et al. 2001, and Briaud et al. 2001). They have found that a more compact or denser fine material will better resist the erosion forces. This contradiction can be explained for the sediments tested in this study, which are a mixture of fine and coarse sizes, by the different bulk density values of the sand and the clay. First of all, consider that the bulk density of pure sand is higher than for clay. In the case of pure clay samples, they become more resistant as their density increases. However, for mixtures of clay and sand material having higher bulk density than clay alone, the critical shear stress may not be higher because of the presence of sand which reduces the interparticle forces. For this reason, bulk density is not a clear predictor variable, and so Equation 4.8 is preferred over Equation 4.9 as a linear model.

In fluid mechanics, the use of dimensionless variables helps to reduce the number of variables, facilitate data analysis, perform fewer experiments, and scale for different dimensions and fluid properties. In this case, the main advantage for nondimensionalizing is that it allows comparison of the results for critical shear stress

with those for uniform coarse sediments using the widely known Shields diagram (Sturm 2001). As shown previously in Chapter 2, the Shields diagram can be placed in the form

$$\tau_{*c} = f(d_*) \tag{4.10}$$

in which τ_{*c} = Shields parameter = $\tau_c/(\gamma_s - \gamma)d_{50}$; and the dimensionless particle diameter $d_* = [(SG - 1)gd_{50}^3/\nu^2]^{1/3}$ where SG = specific gravity of the sediment and ν = kinematic viscosity of the fluid.

Unlike Shields' data, the natural sediment exposed to erosion around bridge foundations is a mixture of both fine and coarse sizes with varying magnitudes of interparticle forces that can affect the comparison. The regression analysis results are shown in Table 4-15 for $log\ \tau_{*c}$ with one of the independent variables taken to be $log\ d_*$ since this is the form in which the Shields diagram is given. The best two-variable predictor model that includes $log\ d_*$ also includes *Fines* content (decimal fraction) as the second variable. This analysis includes all 17 data points and explains the behavior of the sample from McIntosh Co. The regression equation is given by

$$\tau_{*c} = 0.586 \cdot 10^{2.67 \cdot Fines} \cdot d_*^{-0.337} \tag{4.11}$$

as shown by the MINITAB output in Table 4-15. The standard error in the log of the Shields parameter is 0.3 and $R^2 = 0.89$. It is of interest to note that experimental data for

silt size particles (crushed quartz) plots on the Shields diagram with an exponent on d_* of –0.39 which is close to the value found in Equation 4.11 (Sturm 2001).

Table 4-15. MINITAB output showing the best subsets of predictors for logarithm of the Shields parameter as the response.

Best Subsets Regression: LogT* versus Bulk, WC, ...

Response is LogT*

Vars	R-Sq	R-Sq(adj)	Mallows C-p	S	Bulk	WC	OM	d50	Clay	Fines	Log d*
1	88.1	87.3	0.1	0.30473						X	
1	78.4	77.0	10.8	0.41079							X
2	90.6	89.3	-0.7	0.28016	X					X	
2	**89.3**	**87.8**	**0.8**	**0.29971**						**X**	**X**
3	91.2	89.2	0.7	0.28161	X	X				X	
3	91.0	88.9	0.9	0.28500	X			X		X	
4	91.7	89.0	2.1	0.28468	X	X		X		X	
4	91.7	88.9	2.2	0.28481	X	X				X	X
5	92.0	88.3	3.8	0.29244	X	X		X	X	X	
5	92.0	88.3	3.9	0.29261	X	X			X	X	X
6	92.3	87.7	5.5	0.30094	X	X	X	X	X	X	
6	92.3	87.6	5.5	0.30108	X	X	X		X	X	X
7	92.6	86.8	7.2	0.31148	X	X		X	X	X	X
7	92.4	86.6	7.3	0.31388	X	X	X	X	X	X	X
8	92.8	85.5	9.0	0.32613	X	X	X	X	X	X	X

In summary, the best model with two predictors in the form of the Shields diagram (*log* τ_{*c} vs. *log* d_*) includes *Fines* content as an additional parameter. The other model with two predictors in Table 4-15 introduces bulk density which is problematic as described previously. In addition, all of the models with three or more predictors in Table 4-15 provide negligible increases in R^2. Figure 4-4 shows the comparison between the predicted and measured critical Shields parameter using the results of Table 4-15.

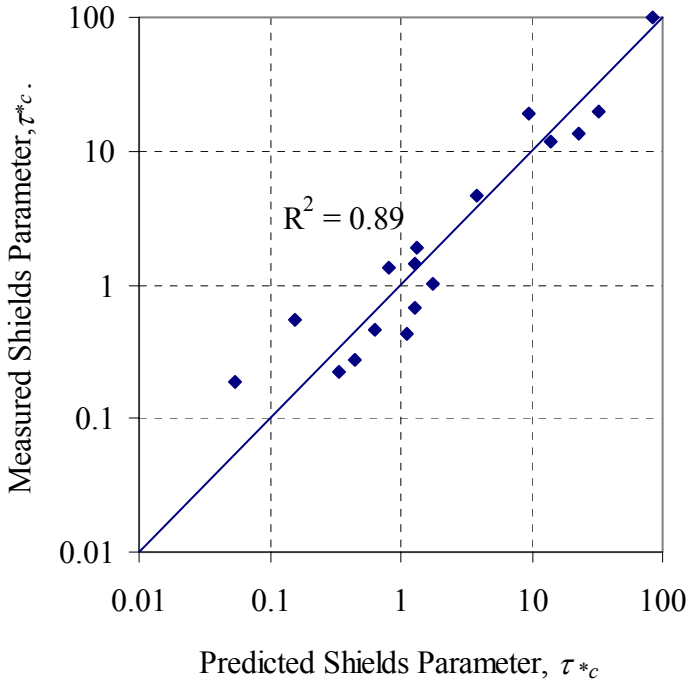

Figure 4-4: Comparison of the measured and predicted critical shear stress parameter using Equation 4.11.

Figure 4-5 shows the results plotted in the Shields diagram. Notice the measured values close to the Shields curve which correspond to sandy material with low fines content. For the special case used to calibrate the flume testing with uniform sand material, which is similar to the material used to develop the Shields curve, the data point falls within the upper range of the Shields curve. Either Equation 4.11 or Figure 4-5 can be used to estimate the critical shear stress value of sediment when its fines content and size are known.

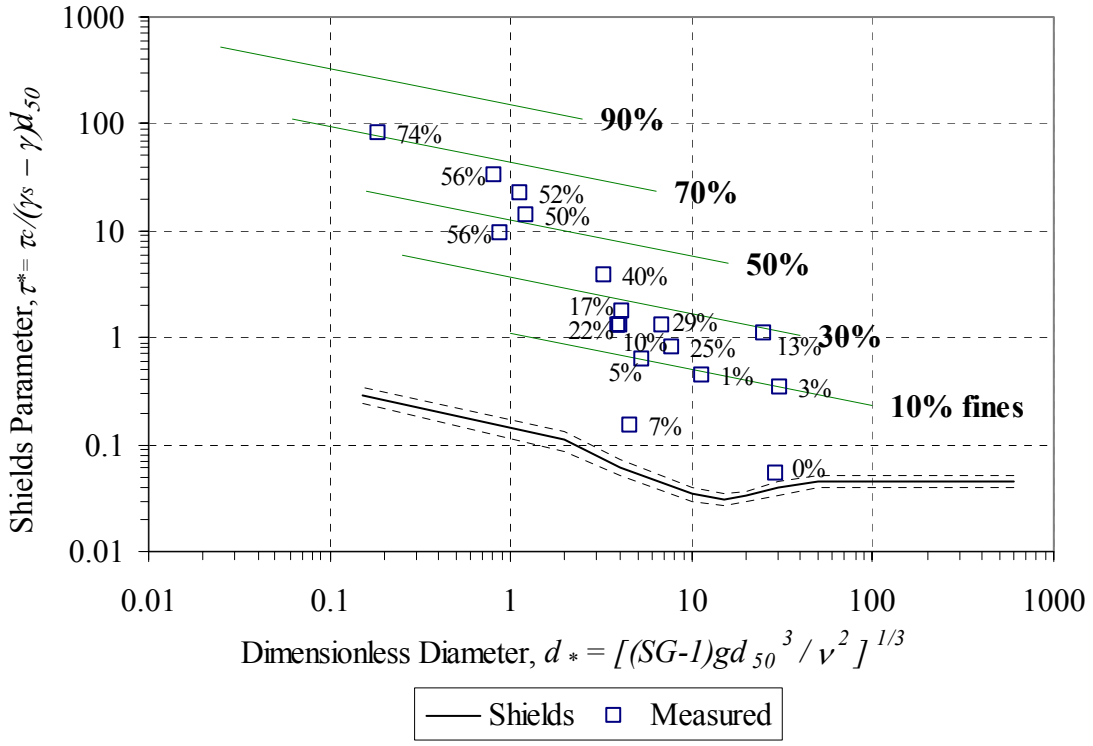

Figure 4-5: Comparison of the measured data and calculated values using Equation 4.11 plotted on Shields' diagram format.

Once the critical shear stress can be estimated, as shown in the preceding analysis, the next step is to relate the erosion rate constant to soil properties. In the following section, the erosion rate constant is analyzed both for the linear part of initiation of motion applicable to low shear stresses and for the exponential model, which describes the erosion response over a wider range of both applied shear stresses and erosion rates.

4.5 Erosion Rate Constant Dependency on Sediment Properties

For excess shear stress relationships, the second parameter of importance is the erosion rate constant. This constant, called "*M*" in the linear case, and "*a*" in the exponential model, quantifies the relative increase in the erosion rate as the response for an increase in the applied shear stress above its critical value. In the linear case, *M* is defined as the erosion rate predicted for an applied shear stress equal to twice the value of the critical shear stress. Possible correlation is also sought using different erosion rate constants expressed by $s_1 = M/\tau_c$, which represents the erosion rate predicted for a unit increment (1 Pa) above the critical shear stress. Similar definitions can be stated for the exponential case. The proposed erosion rate relationship then takes the form

$$E = s_1(\tau - \tau_c) \tag{4.12}$$

for the linear case and for the exponential case it becomes

$$E = E_c e^{s_2(\tau - \tau_c)} \tag{4.13}$$

Equations of this form have been proposed by Lee et al. (1994) and by several other investigators as shown previously in Table 2-2.

Six possible forms of the erosion rate constants are evaluated, and they are given by *M*, s_1, *log* s_1, *a*, s_2, and *log* s_2. They were studied and the predictors that provided the best

explanation for the variability in the erosion rate constants were *Fines*, *log Fines*, d_*, and *log* d_*.

The best expression found for the erosion-rate constant in the linear case is using the logarithm of the response variable, *log* s_1, where s_1 is in (kg/m^2/s)/Pa. The best predictors are the logarithm of the fines content, *log Fines*, where *Fines* is given as a decimal fraction, and the dimensionless particle diameter, d_*., as shown in Table 4-16. The expression is given by

$$s_1 = 0.00191 \cdot Fines^{-1.11} \cdot 10^{0.0305 \cdot d_*} \tag{4.14}$$

which applies for values of *Fines* > 0. The expression given by Equation 4.14 was chosen according to the statistical analysis performed. The regression analysis has a coefficient of determination of R^2 = 0.79, and a standard error in *log* s_1 of 0.42. The measured vs. predicted values of s_1 are shown in Figure 4-6.

Table 4-16. MINITAB output showing the best subsets of predictors for logarithm of s_1 as the response variable.

Best Subsets Regression: logs1 versus Fines, logfines, d*, Logd*

Response is logs1

16 cases used, 1 cases contain missing values

Vars	R-Sq	R-Sq(adj)	Mallows C-p	S	Fines	logfines	d*	Logd*
1	73.4	71.5	2.5	0.46421		X		
1	63.5	60.9	7.9	0.54368	X			
2	**79.5**	**76.3**	**1.2**	**0.42305**		**X**	**X**	
2	77.7	74.3	2.1	0.44083		X		X
3	79.8	74.7	3.0	0.43721		X	X	X
3	79.6	74.5	3.1	0.43864	X	X	X	
4	79.8	72.4	5.0	0.45650	X	X	X	X

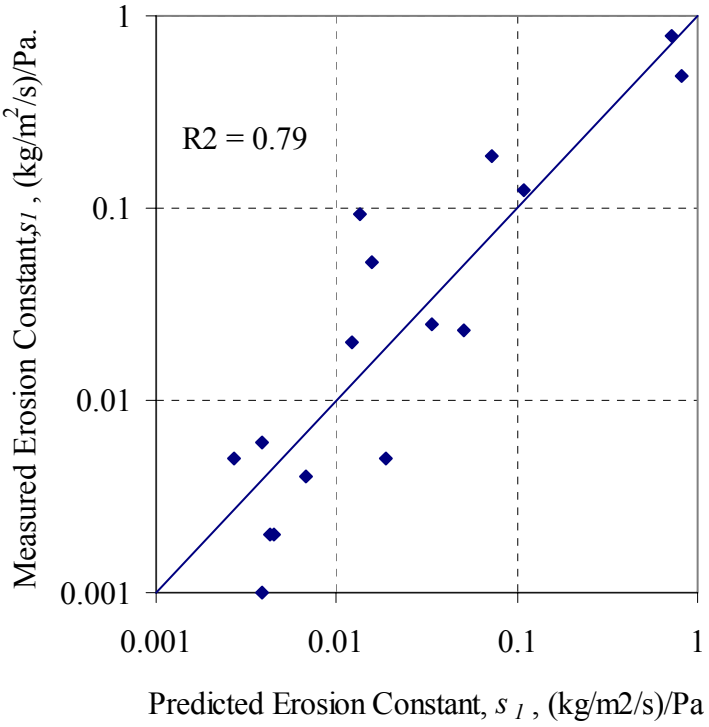

Figure 4-6. Comparison of the measured and predicted erosion rate constant s_1 using equation 4.14.

Figure 4-7 and Equation 4.14 compare the data measured in the lab with the predicted values of the erosion rate constant using a plot similar to the Shields diagram. The dimensionless diameter is plotted on the x-axis, while on the y-axis the erosion constant replaces the value of the dimensionless shear stress. It is of interest to note that the values found by Hoepner (2001) for an estuary mud collected from the Providence River in Rhode Island agree well with the proposed relationship. This material had values of d_* between 0.25 and 0.5, and *Fines* content between 84 and 99%.

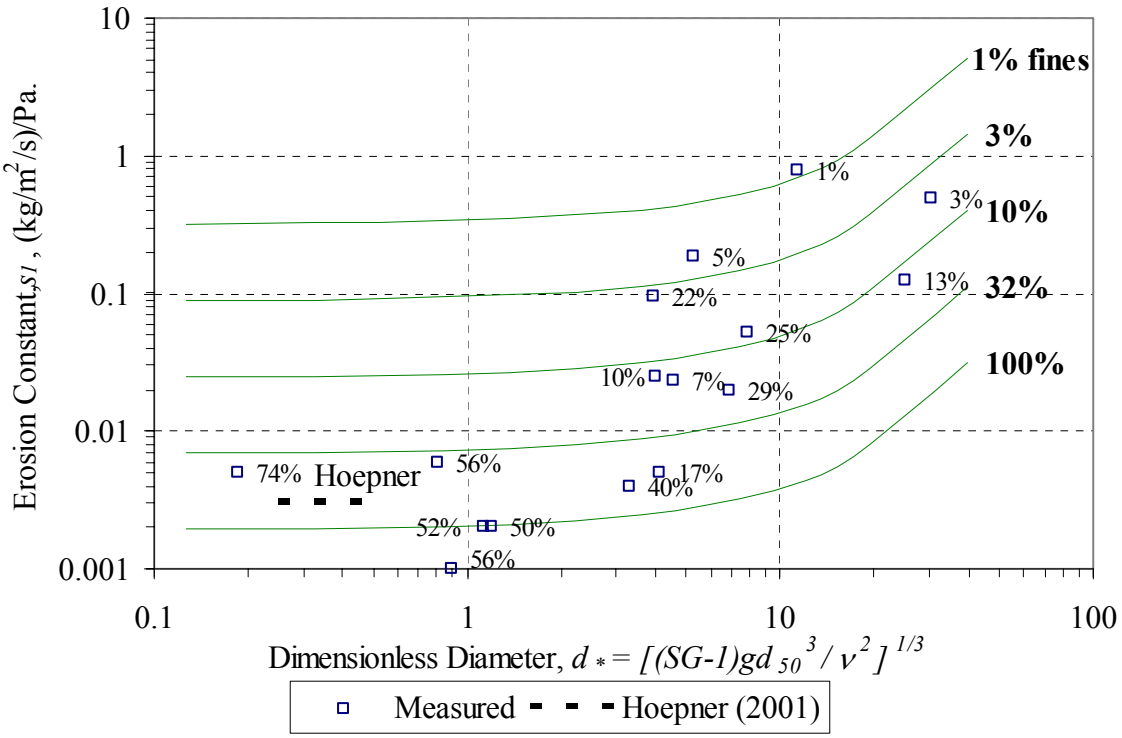

Figure 4-7. Comparison of the measured data and calculated values using Equation 4.14.

Analyzing the results in Figure 4-7, two effects can be described. The first is governed by the fines content. Higher values of fines content increases the resistance to erosion. Consequently, the erosion rate constant is observed to decrease as the fines content increases. On the other hand, once the applied shear stresses go beyond the critical threshold, the erosion rate is dictated by the thickness of the layer to be eroded. That thickness depends on the size of the material, and it is observed that the constant increases as the size increases.

The logarithm of fines transformation in the best-fit relationship depicted in Figure 4-7 gives the same importance to the range of values from 0 to 10% as to the range of values from 10% to 100%. Examples of similar behavior are stated in the soil mechanics literature (Santamarina et al. 2001). For instance, the value of the hydraulic conductivity can drastically change when percent fines is about 7%. Another example is that for values around 10% fines content, the pores of a coarse material can be completely filled.

The best relationship found to estimate the erosion rate constant for the exponential case is linear. This relates the value of s_2 with *Fines* and d_*. This relationship is given by

$$s_2 = 1.44 - 1.60 \cdot Fines + 0.0794 \cdot d_* \qquad (4.15)$$

which applies mostly for materials with *Fines* content higher than 5%. Four out of the thirteen measured relationships between erosion rate and shear stress had a poor

exponential fit. The reduction in the size of the data set affected the uncertainty in the regression model. Details of the best subsets of the predictors are shown in Table 4-17.

Although *Fines* content does not seem to play a very important role according to this model output, it is included as a predictor given that it has shown to be the most important variable in the analysis of both the critical shear stress and the erosion rate constant for the linear model.

Table 4-17. MINITAB output showing the best subsets of predictors for s_2 as the response variable.

Best Subsets Regression: s2 versus Fines, logfines, d*, Logd*

Response is s2

13 cases used, 4 cases contain missing values

Vars	R-Sq	R-Sq(adj)	Mallows C-p	S	Fines	logfines	d*	Logd*
1	69.5	66.7	3.4	0.69276			X	
1	62.3	58.9	6.4	0.77001				X
2	**74.0**	**68.8**	**3.6**	**0.67068**	**X**		**X**	
2	72.7	67.3	4.1	0.68719			X	X
3	76.2	68.3	4.7	0.67654	X	X	X	
3	74.0	65.4	5.6	0.70690	X		X	X
4	80.4	70.6	5.0	0.65170	X	X	X	X

Measured vs. predicted values of the exponential erosion-rate constant s_2 are shown in Figure 4-8, and the results are presented in graphical form in Figure 4-9. The regression relationship seems to follow the same trends as for s_1 shown previously in Figure 4-7.

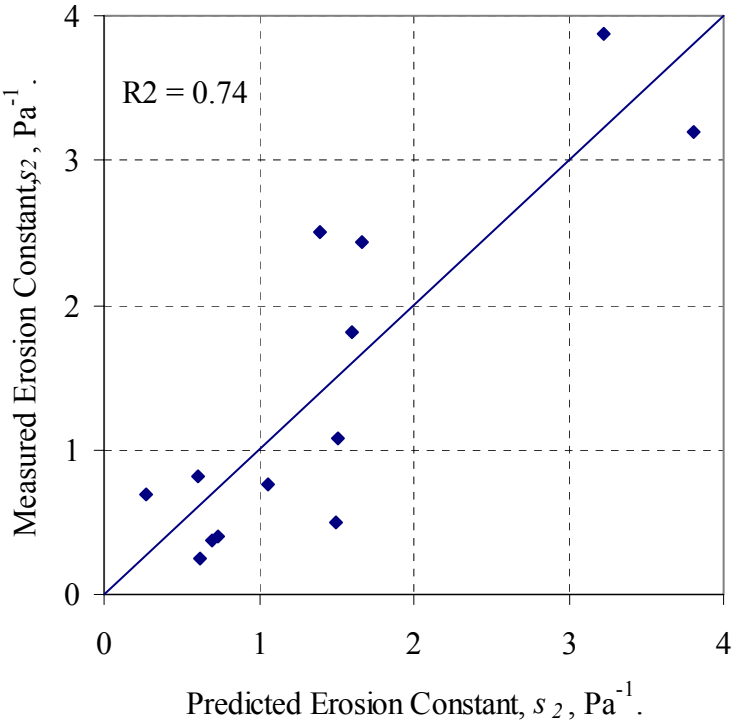

Figure 4-8. Comparison of the measured and predicted erosion rate constant s_2 using Equation 4.15.

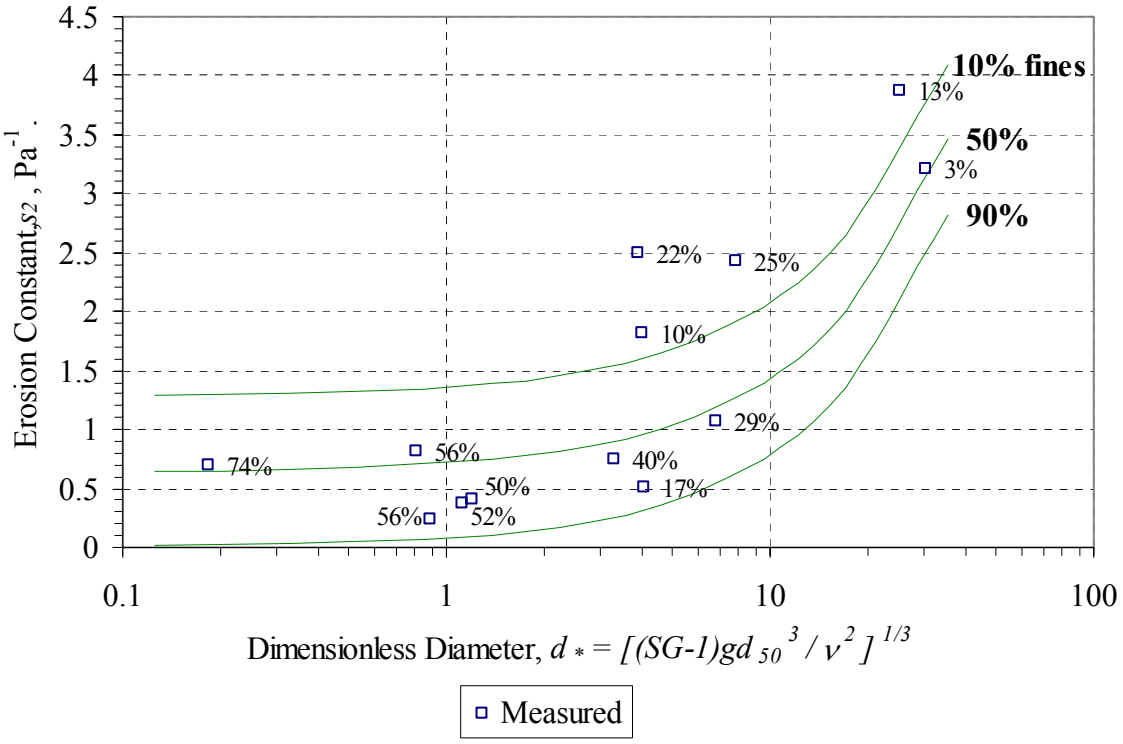

Figure 4-9. Comparison of the measured data and calculated values using Equation 4.15.

It has to be considered, given the limited experiments performed, that this procedure is applicable for sediment collected from similar environments. The material studied came from bridge foundations, material usually consolidated and obtained from 1 to 35 ft deep below the top of the river bed. The relationships that were developed to estimate the critical shear stress and linear erosion rate constant are encouraging. The relationship found for the exponential erosion rate constant is less reliable than the others, but it has the advantage of describing the erosion rate over a wider range.

CHAPTER V

CONCLUSIONS AND RECOMMENDATIONS

5.1 Conclusions

Shelby tube sediment samples collected from the foundations of ten (10) bridges located in the state of Georgia were tested in the laboratory to find their erosional behavior and the correlation of erosion parameters with sediment properties in order to improve the prediction of scour around bridge foundations. These sites were spatially distributed in order to fall into different major river basins and in different physiographic regions. Flume measurements of erosion were performed using a rectangular, tilting, recirculating flume located in the hydraulics lab in the School of Civil and Environmental Engineering at Georgia Tech.

Multiple linear regression analysis was applied to the laboratory erosion data to develop erosion rate relationships as a function of flow conditions and sediment properties for the sediment samples taken at bridge sites in Georgia. Experimental determination was required given the complexity of the phenomenon due to interparticle forces that resist erosion of fine-grained material. The methodology used to describe the erosion phenomenon for this study is to analyze flow conditions and sediment properties separately. First, erosion rates are related to flow conditions characterized by the applied shear stress in the form of excess shear stress relative to the critical shear stress required for initiation of erosion. Second, parameters of critical shear stress and erosion-rate

constant found in the first step are then correlated with sediment properties. Those parameters depend on the regression model that provided the best fit of the data. The two best regression models explored were combined to describe a methodology that can be used to characterize the behavior of a given sediment exposed to specified flow conditions. A linear/piecewise linear model is selected to determine the value of the critical shear stress of the sediment which is then related to its properties. The linear model also describes the behavior of sediment tested under erosive conditions near the critical value, which will produce low erosion rates. An exponential model is suggested to be the best in describing the erosion rate response over the full range of applied shear stress values. However, this broad applicability involves a trade-off in the loss of precision in predicting low erosion rates.

An additional analysis explored in this study is the correlation of the sediment properties, including the erosion parameters, with the geographic origin of the sediment samples within Georgia, although heterogeneity of the sediments even at the same site and in the same physiographic region made trends difficult to identify. Nevertheless, similar structures in the sediment layers near the bridge foundations were observed and documented. In the Valley and Ridge and the Blue Ridge regions, for example, a trend was identified in which material with higher erosional strength is located on top of coarse material with low strength. In addition, materials with high fines content that exhibited high resistance to erosion appeared repeatedly in the Coastal Plain region.

Critical shear stresses for the consolidated sediments tested in this study ranged from approximately 0.5 Pa to greater than 21 Pa. For comparison, most previous studies have focused on pure clays with limited settling time having critical shear stresses of the order of 1 Pa. The sediment samples tested in this study have a wide range of sizes from pure sands to almost pure clay and many mixtures in between. Erosion testing of these naturally occurring materials produces a methodology applicable to the observed wide range in sediment sizes. Of course, this wide range of applicability sacrifices precision that can be reached by methods developed for more specific cases, such as coarse sediments or pure clays. For these naturally occurring mixtures, fine material content is found to have an enormous influence and appears as the best predictor in most of the regression models selected. This influence shows indirectly the contribution of interparticle forces to the erosion process.

5.2 Suggested Modifications to the Procedure

The main suggested modification is to implement a slightly different experimental design for sediments that are highly heterogeneous. The present study focused on finding the critical shear stress of the sediment samples by starting with low applied shear stresses near the critical value and increasing the shear stresses to determine erosion rates as a function of applied shear stress. In some instances, the sediment layer was completely eroded before higher shear stresses could be applied. It would be desirable to measure erosion rates over a wider range of shear stresses by knowing in advance the thickness of the sample layer available to be eroded. In order to accomplish this, identification of the material to be tested is required in order to adjust the experimental plan to be followed in

the laboratory. Among the options that may be possible are a nonintrusive examination of the Shelby tube material or collection of two sample tubes at the same height, one for sediment property tests and the other for the flume test.

5.3 Suggested Future Research

Future research should include a review of available erosion data to augment the present data set, although most previous studies have focused on either pure clay samples or pure uniform sands. Also, additional measurements of the erosion properties of sediment composed of a mixture of sizes would be helpful in obtaining a more comprehensive data set for analysis. A set of guidelines should be established for erosion properties that would include not only a global definition of critical shear stress, but also specification of minimum and maximum erosion rates for different types of sediments and critical shear stress ranges for these sediment types.

REFERENCES

Alhadeff, S. J., Musser, J. W., Sandercock, A. C., and Dyar, T. R. (2000). "Digital Environmental Atlas of Georgia." *Georgia Geologic Survey Publication CD-1.* U. S. Geological Survey and Georgia Department of Natural Resources. 2 Disks.

Ariathurai, R., and Arulanandan, K. (1978). "Erosion rates of cohesive soils." *J. Hydraulic Eng.,* 104(2), 279-283.

Arulanandan, K., Loganathan, P., and Krone, R. B. (1975). "Pore and eroding fluid influences on surface erosion of soil." *J. Geotech. Eng.,* 101(1), 51-66.

Arulanandan, K., and Perry, E. B. (1989). "Erosion in relation to filter design criteria in earth dams." *J. Geotech. Eng.,* 109(1), 682-698.

Black, K. S., Tolhurst, T. J., Paterson, D. M., and Hagerthey, S. E. (2002). "Working with natural cohesive sediments," *J. Hydraulic Eng.,* 128(1), 2-8.

Briaud, J. L., Ting, C. K., Chen, H.C., Gudavalli R., Perugu, S., and Wei, G. (1999). "SRICOS: Prediction of scour rate in cohesive soils at bridge piers," *J. Geotechnical and Environmental Eng.,* 125(4), 237-246.

Briaud, J. L., Ting, C. K., Chen, H.C., Cao, Y., Han, S. W., and Kwak, K. W. (2001). "Erosion Function Apparatus for Scour Rate Prediction." *J. Geotechnical and Environmental Eng.,* 127(2), 105-113.

Chen, N. S., Chiew, Y. M. (1999). "Analysis of initiation of sediment suspension form bed load." *J. Hydraulic Eng.*, 125(8), 855-861.

Chen, N. S., (2002). "Exponential formula for bedload transport." *J. Hydraulic Eng.*, 128(10), 942-946.

Hoepner, M. A. (2001). "Stability of cohesive sediments from flume and rheometer measurements." Masters thesis, Georgia Institute of Technology, Atlanta, GA.

Hunt, S. D., and Mehta, A. J. (1985). "An evaluation of laboratory data on erosion of fine sediment beds." *Particulate and multiphase processes, vol. 3: Colloidal and interfacial phenomena,* Hemisphere, Washington, D. C., 503-518.

Israelachvili, J. (1992), "Intermolecular and surface forces." *Second edition, Academic Press*, London, 450 pp.

Julien, P. Y. (1995), "Erosion and Sedimentation." *Cambridge University Press*, New York, 280 pp.

Kamphuis, J. W., Hall, K. R. (1983), "Cohesive material erosion by unidirectional current." *J. Hydraulic Eng.*, ASCE, 109(1), 49-61.

Kandiah, A. (1974). "Fundamental aspects of surface erosion of cohesive soils." PhD thesis, University of California, Davis, Calif.

Krone, R. B. (1999). "Effects of bed structure on erosion of cohesive sediments." *J. Hydraulic Eng.*, 125(12), 1297-1301.

Langendoen, E. J. (2000). "CONCEPTS – Conservational channel evolution and pollutant transport system: Stream corridor version 1.0." *Research Report No. 16,* US Department of Agriculture, Agricultural Research Service, National Sedimentation Laboratory, Oxford, MS.

Lee, S. C., Mehta, A. J., and Parchure, T.M., (1994). "Cohesive sediment erosion: Part I, test devices and field instrument assemblies. Part II, relationship between the erosion rate constant and bed shear strength." *Internal Report*, Coastal and Oceanographic Engineering Dept., University of Florida, Gainesville, Fla.

Mahmood, T., Amirtharajah, A., Sturm, T. W., and Dennet, K. E. (2001). "A micromechanics approach for attachment and detachment of asymmetric particles." *Colloids and Surfaces: A. Physicochemical and Engineering Aspects*, 177, 99-110.

Mazurek, K. A., Rajaratnam, N., and Sego, D. C., (2001). "Scour of cohesive soil by submerged circular turbulent impinging jets," *J. Hydraulic Eng.,* 127(7), 598-606.

McNeil, J., Taylor, C., and Lick, W. (1996). "Measurements of erosion of undisturbed bottom sediments with depth." *J. Hydraulic Eng.*, 122(6), 316-324.

Mehta, A. J., and Partheniades, E. (1975). "An Investigation of the depositional properties of flocculated fine sediments." *J. Hydraulic. Research*, 12(4), 361-381.

Mehta, A. J., Parchure, T. M., Dixit, J. G., and Ariathrai, R. (1982). "Resuspension potential of deposited cohesive beds." *Estuarine comparisons*, Academic, New York.

Mehta, A. J., and Partheniades, E. (1982). "Resuspension potential of deposited cohesive sediment beds." *Proc., 18th Coast Eng. Conferences,* Vol. II, ASCE New York, 1569-1588.

Mehta, A. J., Hayter, E. J., Parker, W. R., Krone, R. B., and Teeter, A. M. (1989). "Cohesive sediment transport. I: Process Description." *J. Hydraulic. Eng.*, ASCE, 115(8), 1076-1093.

Mehta, A. J. (1991). "Characterization of cohesive soil bed surface, with special reference o the relationship between erosion shear strength and bed density," *Report No.* UFL/COEL.MP-91/4, Coastal and Oceanographic Engineering Dept., University of Florida, Gainesville, Fla.

McNeil, J., Taylor, and C., Lick, W. (1996). "Measurements of erosion of undisturbed bottom sediments with depth," *J. Hydraulic Eng.,* 122(6), 316-324.

Otsubo, K., Murakoa, K. (1988). "Critical shear stress of cohesive bottom sediments." *J. Hydraulic Eng.,* 114(10), 1241-1256.

Parchure, T. M., and Mehta, A. J. (1985). "Erosion of soft cohesive sediment deposits." *J. Hydraulic. Eng.*, 111(10), 1308-1326.

Partheniades, E. (1965). "Erosion and deposition of cohesive soils," *J. Hydraulic Eng.,* 91(1), 105-139.

Ravens, T. M. and Gschwend, P. M., (1999). "Flume measurements of sediment erodibility in Boston Harbor," *J. Hydraulic Eng.,* 125(10), 998-1005.

Ravisangar, V. (2001). "The role of sediment chemistry in stability and resuspension characteristics of cohesive sediments." Ph.D. Thesis, Georgia Institute of Technology, Atlanta, GA.

Ravisangar, V., Dennet, K. E., Sturm, T. W., and Amirtharajah, A. (2001). "Effect of sediment pH on resuspension of kaolinite sediments," *J. Environmental Eng.,* 127(6), 531-538.

Ravisangar, Sturm, T. W., and Amirtharajah, A. (2004). "Influence of sediment structure on erosional strength and density of kaolinite sediment beds," Approved for publishing *J. Hydraulic Eng.*

Richardson, E. V., and Davis, S. R. (2001). "Evaluating scour at bridges" *Report HEC-18,* 4th Edition, U.S. Federal Highway Administration, May.

Roberts, J., Jepsen, R., Gotthard, D., and Lick, W. (1998). "Effects of particle size and bulk density on erosion of quartz particles." *J. Hydraulic Eng.*, 124(12), 1261-1267.

Roberts, J.D., Jepsen, R. A., and James, S. C. (2003). "Measurements of sediment erosion and transport with adjustable shear stress erosion and transport flume." *J. Hydraulic Eng.*, 129(11), 862-871.

Santamarina, J. C., Klein, K. A., Fam, M. A. (2001). "Soils and waves," *John Wiley and Sons Ltd.,* England, 488 pp.

Santamarina, J. C. (2001). "Soil behavior at the microscale: particle forces," *Proc. Symp. Soil behavior and soft ground construction, in honor to Charles C. Ladd,* MIT, 1-32.

Shields, A. (1936). "Applications of similarity principles and turbulence research to bed-load movement." *Hydrodynamics Laboratory Publ. No. 167,* trans. W. P. Ott and J. C. van Uchelen. Pasadena: USDA, Soil Conservation Service Cooperative Laboratory, California Institute of Technology..

Sowers, G. F. (1979). "Introductory soil mechanics and foundations." *Macmillan, Fourth Edition,* New York, 621pp.

Spork, V., Ruland, P., and Rouve, G. (1995). "Modeling sediment transport in a river reservoir with parameters measured in an annular flume." *6th International Symposium on River Sedimentation,* 599-606.

Sturm, T. W. (2001). "Open channel hydraulics." *Textbook series in water resources and environmental engineering, McGraw Hill,* New York, 493pp.

Ting, F.C., Briaud, J. L., Chen, H. C., Gudavalli, R., Perugu, S., and Wei, G. (2001). "Flume tests for scour in clay at circular piers," *J. Hydraulic Eng.,* 127(11), 969-978.

van Olphen, H. (1977). "An introduction to clay colloid chemistry," *second edition, John Wiley & Sons,* New York, 318 pp.

Zreik, D.A., Krishnappan, B. G., Germaine, J. T., Madsen, O. S., and Ladd, C. C. (1998). "Erosional and mechanical strengths of deposited cohesive sediments." *J. Hydraulic Eng.,* 124(11), 1076-1085.